8 Pre-chamber Ignition 2

8.1 Characterization of the Ignition and Early Flame Propagation of Pre-Chamber Ignition System in a High Pressure Combustion Cell

Marcus Wöbke, Paul-Benjamin Reinicke, Michael Rieß,
Lorenz von Römer, Marc Sens

Abstract

The Pre-Chamber spark plug, already in its most simple configuration, allows a cycle fuel consumption reduction of 2-3% (WLTC) by enabling a significant compression ratio increase due to its huge knock mitigation effect. This benefit can be strongly extended in the homogeneous lean burn operation mode with very low nitrogen oxide emissions by a novel approach of injecting a well prepared fuel-air-mixture inside the Pre-Chamber. An increase of the engine compression ratio allows further the development of a new combustion process referred as the Pre-Chamber supported self-ignition process, which enable an increased thermodynamic efficiency at part load operating points of a gasoline engine.
The development of a suitable Pre-Chamber ignition system requires the technical understanding of the Pre-Chamber geometry parameters on the combustion process. The impact of the overflow channel design on the flame propagation and ignition of the fuel-air mixture inside the main chamber must be understood in greater detail. This in turn requires a high-fidelity combustion model which is capable of predicting the impact of the overflow channel geometry on e.g. flame extinction, radical recombination on the walls of the Pre-Chamber orifice and finally the behavior of main chamber inflammation regardless of the Pre-Chamber ignition regime.

Focus of this work is to discuss the impact of the Pre-Chamber geometry onto the inflammation and early flame propagation inside the main combustion chamber by means of experiments in an optical high pressure vessel under simplified boundary conditions. As a basis, the simultaneous high speed measurement of Schlieren and OH* chemiluminescence serve as a fundamental means to analyze ignition performance and early flame propagation in order to develop and validate an accurate combustion model.

Initially, the general impact of the chamber pressure will be discussed emphasizing specifically on the differences between certain Pre-Chamber layouts and the conventional ignition system onto flame speed and ignition probability. Furthermore, variations of e.g. the number of overflow holes, the orifice diameter and the volume of the Pre-Chamber aids to identify the most relevant parameters responsible for flame extinction and combustion performance inside the main chamber.

1 Introduction

1.1 Motivation

Latest and future legislations for automotive emission of pollutants and CO_2 are forcing the industry to develop highly efficient powertrain concepts. As a result, the electrification of powertrains has become a main industry trend and a very promising approach for drastically reducing the local emissions. However, today´s most likely scenario for future powertrains still incorporates the internal combustion engine with varying vigorousness, admittedly not as mere propulsion system (ICE only), but with a major share in combination with light (xHEV) or rather powerful (PHEV) electrification (see Figure 1.1). Consequently, the optimization of the ICE in both terms, efficiency and pollutant emissions is crucial for competing against powertrains with locally zero emissions.

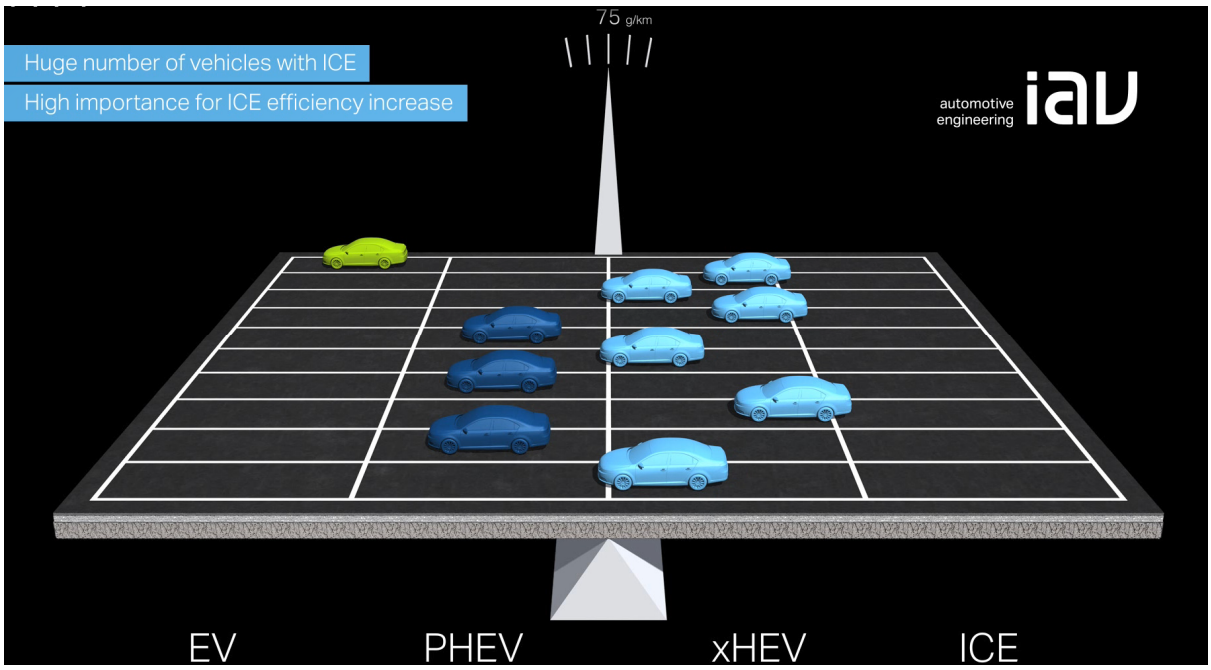

Figure 1.1: IAV's powertrain-share fleet scale with one exemplary prediction of the powertrain mix in 2025 - 2030

During the last 20 years, the ICE passed through a comprehensive development with already considerable improvement of fuel efficiency. Further optimizations become more and more complex and expensive. Several technologies are known with theoretical high potential for reduction of process related efficiency losses such as early intake valve closure (EIVC) strategies or high mixture dilution. However, they come along with system specific drawbacks that limit the full fuel saving potential. For example, a severe mixture dilution with EGR has a positive impact on reducing the throttle losses in part load and knock sensitivity in high load. However, the engine suffers from a deterioration of mixture inflammability and burn rate caused by the increase of inert gas content.
An advanced ignition system as the Pre-Chamber Spark Plug (PCSP) was shown to be a beneficial complementary technology or even act as an enabler for such high potential ICE technologies [1, 24]. Compared to conventional spark plugs the ignition energy of the PCSP increases by more than two orders of magnitude. Furthermore,

the multiple ignition sources, represented by the flame / hot gas jets from the Pre-Chamber lead to a significantly higher mixture coverage approaching a spatial ignition. To summarize, previous publications indicate a great fuel saving potential [1, 24] which makes the PCSP component a very interesting technology – also and specifically because it is relatively easy to integrate into an engine in terms of packaging / costs and supports various combustion systems in its performance.
However, the layout of the Pre-Chamber itself needs to be accurately matched to the needs of the specific engine and its combustion system. Thus, it is of major importance to understand in detail the influence of the numerous Pre-Chamber design parameters (volume, A/V, hole size, surface, material, etc.) onto the inflammation within the Pre-Chamber and subsequently inside the main combustion chamber also under varying boundary conditions, e.g. from engine cold start up to full load operation. These differing boundary conditions demand a compromise layout of the Pre-Chamber, which in turn shall clearly be the optimum one.
A major requirement for approaching the optimal design and an efficient combustion development work, specifically for PCSP based systems with the numerous influencing parameters, is the application of high-fidelity models that enable predictive simulation of the combustion process.
This paper sets out to describe the work performed within an all-embracing PCSP engine development activity, aiming specifically at in-depth explanation of results from combustion bomb experiments. Clearly, these results are used not only to build a thorough understanding of the combustion process, but also to setup and calibrate an accurate combustion model. The latter will be realized in 3D CFD using CONVERGE software including an advanced chemistry solver to describe in detail Pre-Chamber phenomena, such as flame quenching inside the Pre-Chamber bores because of radical recombination on the channel walls, heat withdrawal and reaction-kinetic behavior (see Figure 1.2). The part explaining the virtual development of this overarching scientific work describing Pre-Chamber combustion will be reported in future publications.

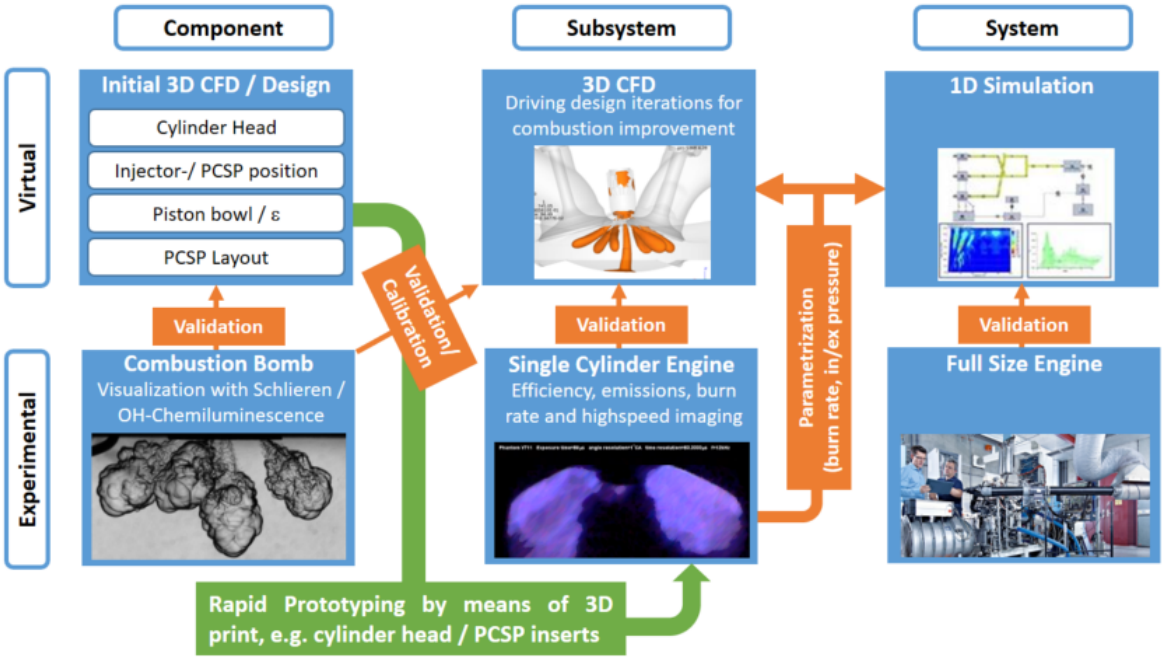

Figure 1.2: Process for Assessment and Development of a PCSP combustion system [24]

1.2 Previous Findings with passive PCSP

Previous investigations of the PCSP on a single cylinder research engine with different complementary technologies, as external cooled EGR and early intake valve closure, show a significant impact of the Pre-Chamber layout to the mixture inflammation and burn rate in the main combustion chamber – especially under critical engine operation conditions [1, 24].
The PCSP ignition system revealed a distinct potential for knock mitigation and thus enabled an increase of compression ratio by 2 to 2.5 units at constant combustion phasing. In-cylinder high speed imaging confirmed the theory of a spatial ignition approach with multiple inflammation zones. In combination with the high ignition energy the PCSP ignition lead to a marked reduction of the pre-reaction time for self-ignition inside the unburnt gas mixture due to shortened ignition delay and combustion duration. Figure 1.3 shows the comparison of combustion parameters for a conventional spark plug and a PCSP system at 2000rpm / 16bar BMEP (knock limited operating point) for two different geometric compression ratios.

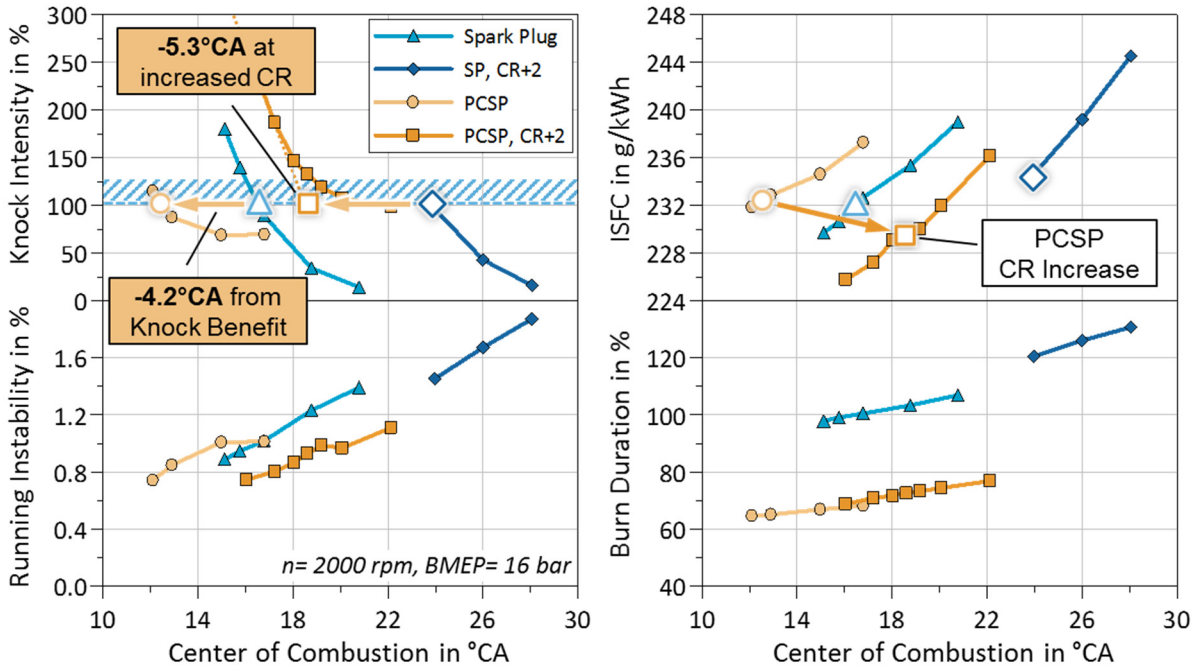

Figure 1.3: Knock mitigation potential of a PCSP compared to a conventional spark plug system for two different compression ratios (10 and 12) [1]

Beside the spacious mixture coverage, the penetrating gas jets of the PCSP generate a high level of turbulence in the main combustion chamber. Both have been found to be very beneficial for the complementary technologies external cooled EGR and EIVC operation – compensating the negative effects by high inert gas fraction and reduced charge air motion, respectively. The grade of improvement possible by the Pre-Chamber ignition system is strongly depended on many different parameters of the PCSP (geometry, material, system integration, etc.). The single cylinder engine investigations in [1] and [24] revealed a mutual interference of these geometrical parameters (e.g. A/V, bore layout, volume, spark location, etc.) on combustion performance on the one hand. On the other hand, certain operating conditions require for example an opposing design of the Pre-Chamber so that the final PCSP layout can only be a compromise.

Especially for engine cold start and high load operation, the requirements for the Pre-Chamber layout seem to be quite conflicting.
Figure 1.4 illustrates the emitted visible light (luminescence) from the in-cylinder combustion (visible optical spectrum) for different PSCP designs, utilizing a high speed camera. The upper row shows the initial phase of combustion with a layout “A” – optimized for high knock mitigation and reduction of fuel consumption in part load – at CA50 of 8°CA (left) and retarded ignition timing (right). Whilst at MBT (Maximum Brake Torque) timing all flame jets, central and lateral, are observed well-distributed inside the main chamber, for late combustion phasing no flames at all are visible. This means, with this PCSP configuration a catalyst heating operation is not possible. The bottom row shows the same comparison with a modified PCSP layout “B” – based on layout “A” with increased central bore diameter.

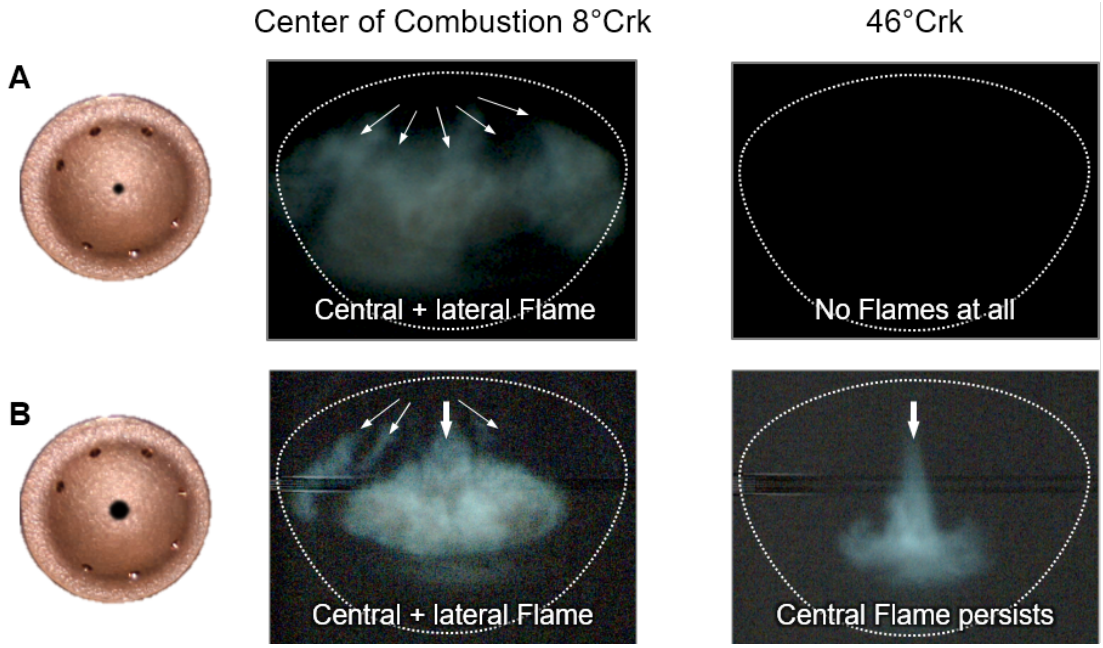

Figure 1.4: High speed camera images from single-cylinder engine: visible light spectrum luminescence of combustion at 1250rpm / 2bar BMEP, two Pre-Chamber variants at base and very late center of combustion [24]

At MBT timing there is a very strong flame jet from the central bore compared to the lateral ones. When retarding the combustion to a CA50 of 46°CA with correspondingly decreasing pressure and temperature, the lateral jets disappear while the jet out of the big central bore still sustains.
Figure 1.5 classifies the two PCSP designs “A” and “B” in a scattering band of various Pre-Chamber layouts in terms of their specific catalyst heating capability. The defined “geometric ratio” represents a multivariate parameter space (containing i.a. A/V, number of bores, bore layout, bore diameter, etc.). It indicates contrary trends for improving the catalyst heating operation and decreasing the knock mitigation potential for example.
The single cylinder engine experiments in [24] identified a further key challenge at the optimization of the Pre-Chamber design. The PCSP comes along with two system specific additional types of wall heat losses, which directly affects the indicated efficiency. One type of heat transfer results mainly from the additional surface of the Pre-Chamber contributing to the total combustion chamber surface. Here, relevant optimization levers are Pre-Chamber material and system integration inside the cylinder head. The

second type of specific wall heat losses is caused by the flame jets of the PCSP. The locally induced turbulence along the jets lead to a significant increase of heat transfer to the main chamber walls – especially at high load. Besides an adjusted flame jet targeting, an optimization of the Pre-Chamber bore geometric parameters could help to avoid direct wall contact and to decrease turbulence close to the walls. For this, a detailed understanding of the impacts of the different parameters to the jet formation and penetration is of particular importance.

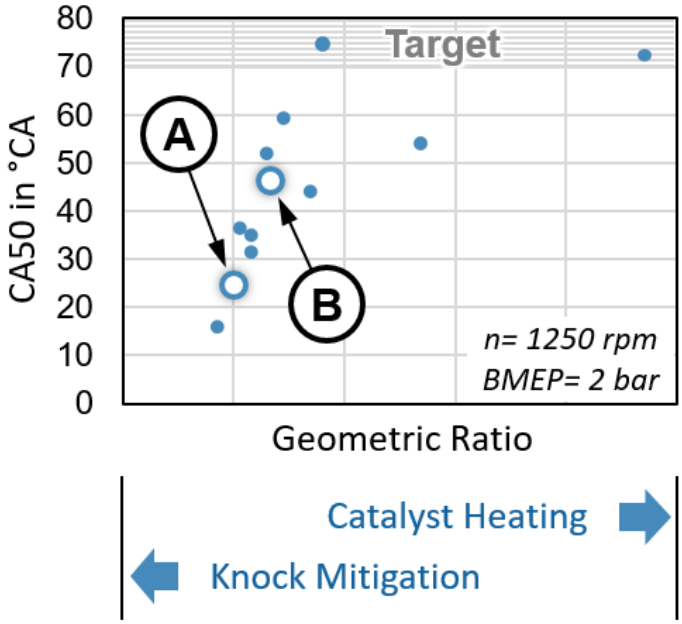

Figure 1.5: Latest possible CA50 across the Pre-Chamber specific geometric ratio for different PCSP layouts at 1250rpm / 2bar BMEP [24]

In the light of the main conclusion of the above described single cylinder engine experiments, some basic thermodynamic considerations shall be stated on a high level in order to better understand the design and result trade-off between low engine load in cold conditions (e.g. catalyst heating) and performance at high load / high temperature (e.g. knocking combustion at boosted operation).

Concerning the conditions inside the combustion chamber, engine cold start clearly poses the most severe challenge for robust inflammation of the main combustion chamber with the Pre-Chamber ignition system. As can be seen in Figure 1.4, it is preferable to enter the regime of flame jet ignition, which means that the flame initiated within the Pre-chamber does not extinguish when passing through the Pre-Chamber orifice. While reasoning as to why this regime is preferable e.g. for engine cold start, the underlying phenomena decisive for either flame or hot gas jet regime shall be discussed first.
Ultimately, the heat loss from the flame to the surrounding walls is the major driver for the flame to extinguish. Referring to what is known as quenching distance, which describes the minimum distance that a flame can propagate through, this parameter is – among others – crucial also for the layout of the Pre-Chamber. Once the flame approaches the orifice, an increasing heat flux to the walls prevents all reactions with high activation energy from being self-sustainable due to an insufficient temperature level. Due to the latter, specifically chain-branching reactions come to a halt so that only

radical recombination reactions are able to take place. Finally, this might lead to ceasing reactions and thus flame quenching [27].
Literature tells that quenching distance is in first order dependent on laminar flame thickness [25, 26, 27] and shows a proportional correlation.
Figure 1.6 in turn shows the dependency of laminar flame thickness on pressure and unburned temperature for a stoichiometric methane/air mixture.

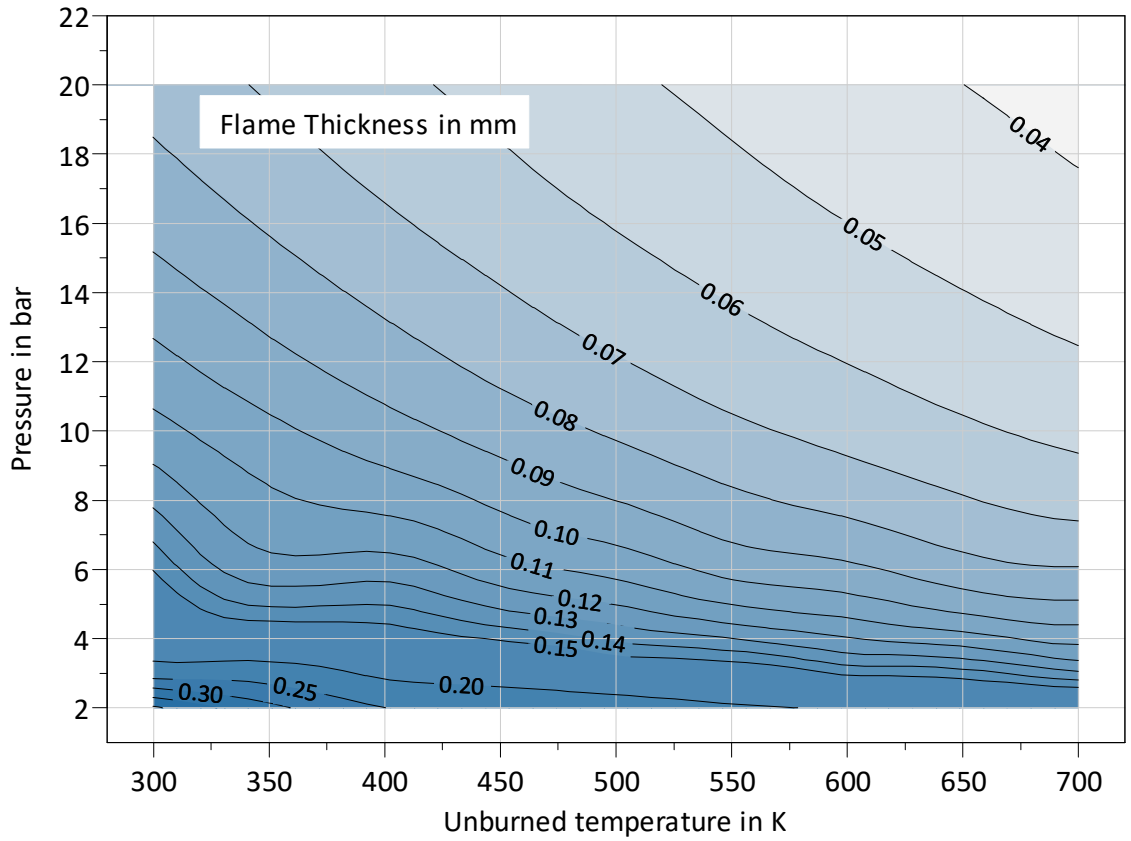

Figure 1.6: Laminar flame thickness dependent on pressure and unburned temperature, calculated at lambda = 1 / EGR = 0% with GRI3.0

It is obvious from the diagram that a decreasing temperature and pressure in the chamber results in a higher flame thickness. Consequently the orifice needs to be bigger to ensure a flame passing through the channel. This behavior is also consistent with observations of Biswas et.al. [25], who could show in combustion bomb experiments that the ignition mechanism shifts from jet ignition regime to flame ignition at increasing pressures.
As for the hot jet ignition regime, the jet consists only of combustion products as the flame has ceased to exist while travelling through the chamber orifice.
Still, a jet of hot gas entering the main combustion chamber is capable to ignite the main chamber mixture even though the number of active radicals it contains is clearly reduced compared to the flame jet regime. Consequently, dominating parameters for the inflammation of the main chamber mixture by hot gas jets is the temperature and mixture of the bulk gas and temperature and the integral turbulence length scale of the hot gas jet. Dependent on the pressure ratio of pre-/and main chamber, the outflow velocity and thus the turbulence level of the hot gas jet is a crucial parameter. In case the turbulence level of the hot gas jet increases so much that the vortexes get as small as the reaction zone thickness, the convective and highly turbulent eddies might cut-

off potential reaction partners from the reaction zone before a self-sustainable chemical reaction is achieved. Increased mixing of cold and unburned mixture with hot reactive gas might lead to local, and in extremum to global quenching of the flame [26], which ultimately results in misfire.

The above described previous findings arise a couple of further questions to the complex interactions of the various Pre-Chamber parameters and their impacts onto the combustion process in the main chamber, that need to be understood in detail for an optimal matching of the PCSP design:

- Impact of total orifice cross section area at constant A/V on combustion performance
- Impact of bore diameter to flame jet structure and penetration as well as turbulent fine structure
- Impact of spark location and bore layout (A/V, bore diameter) to pressure increase inside PCSP
- Impact of spark location and bore layout (A/V, bore diameter) to inflammation delay and flame propagation inside main chamber
- Impact of pressure at ignition to jet penetration
- Impact of A/V or bore diameter to flame extinction
- Impact of ignition regime on inflammation and burn duration in main chamber
- Existence of operating point specific advantages for either flame or hot gas ignition

The present paper tries to examine and answer these questions in the following chapters.

2 High Pressure Combustion Cell

The experimental setup is illustrated in Figure 2.1. The cylindrical steel high pressure combustion cell has a main chamber volume of 2.2 dm^3 and is equipped with 4 circular (diameter 50 mm) quartz windows arranged perpendicular to the spark plug longitudinal axis. A fifth window with a circular quartz window (diameter 100 mm) is located on the opposite side of the spark plug. The modular IAV Pre-Chamber ignition system design known from [1] was used to investigate a broad range of different Pre-Chamber configurations: e.g. volume, spark plug location and the layout of the overflow channels. This modular ignition system insert also enables the use of a conventional M12 spark plug for comparative measurements of the early flame propagation under dormant flow conditions. The ratio of the Pre-Chamber volume to the main chamber volume is around 0.07% and thus much smaller than in a typical engine application (around 2-3%).
The air/fuel mixture inside the combustion cell was heated up to 398 K by eight built-in heating cartridges with a system power of 2800 W integrated in the main chamber walls. To ensure a homogeneous temperature and small natural convection effects of the mixture, four thermocouples (type K) were positioned at the top and on the bottom of the main chamber inside the combustion cell.
The fuel (CH_4 of 99.5% pureness) and the synthetic air (20.5 Vol-% O_2 / 79.5 Vol-% N_2) are injected into the main chamber using the partial pressure method. To ensure a homogeneous mixture in the main chamber and the Pre-Chamber, the gases were injected by two nozzles, one pointing directly at the overflow channels and the other having a swirl element to improve the mixture preparation and homogenization. In preliminary investigations the resting time after the gas being injected was varied between 30 seconds and 10 minutes to study the impact on the combustion process. It was found that a resting time of 2 minutes is enough to gain a homogeneous mixture in the area of optical access. The observed spherical flame propagation induced by a conventional spark plug under different ignition pressure conditions confirms this hypothesis. After each test the combustion cell was drained by a vacuum pump and vented by compressed air to ensure the complete discharge of residual combustion products. The mechanical durability of the combustion vessel limits the maximum peak pressure to 100 bar. This allows a maximum ignition pressure of 18 bar. The mixture inside the Pre-Chamber was ignited by a series production M10 spark plug. The ignition coil was a Delphi Ion sense coil with an ignition energy of 95 mJ and a break down voltage of approx. 23 kV. The spark location and the Pre-Chamber volume was varied by adapter sleeves between the spark plug and Pre-Chamber body. The transient pressure traces were recorded by Kistler 6041B water cooled pressure transducer inside the main chamber and an AVL GH12d pressure transducer inside the Pre-Chamber combined with two Kistler 5018A charge amplifiers. A piezo-resistive Kistler 4045A50 pressure transducer with a Kistler 4603 piezo-resistive amplifier provides the absolute pressure for the piezo electric pressure sensors prior to ignition and is used for the filling of the combustion bomb based on the partial pressure method.

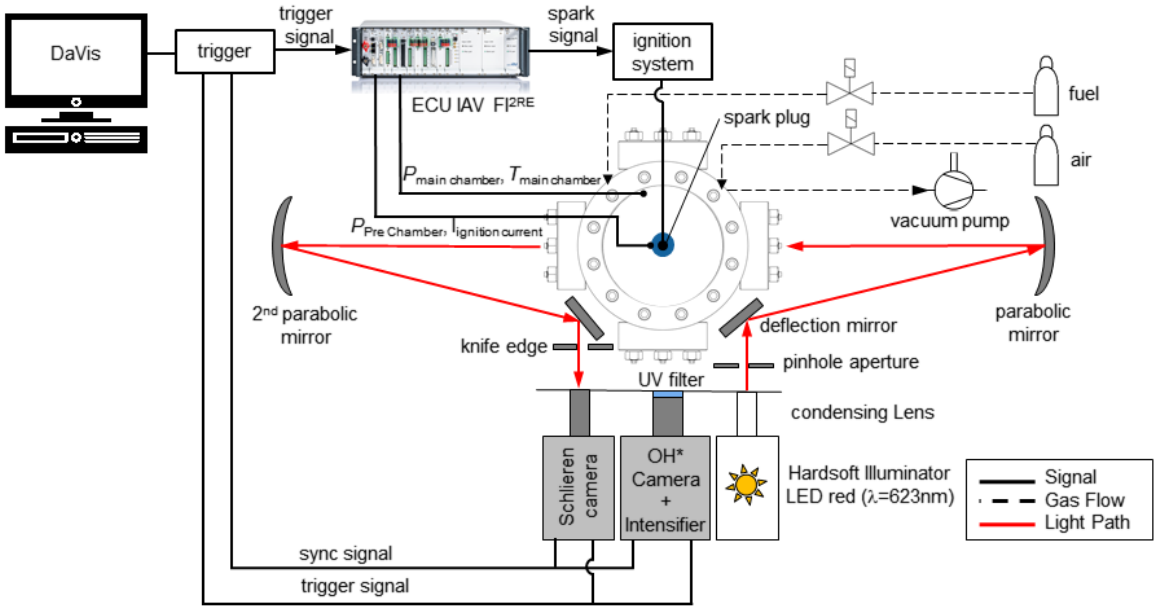

Figure 2.1: Schematic of experimental setup for ignition of premixed methane/air mixture with Pre-Chamber spark plug and conventional spark plug ignition system

2.1 High speed Schlieren and OH* chemiluminescence imaging

The LaVision imaging processing software DaVis with a high-speed controller synchronized and used for triggering the high-speed cameras, the image intensifier and the flexible IAV FI^{2RE} engine control unit. The ECU is equipped with an additional measurement data acquisition card that records the transient pressure traces, the ignition current, the camera triggers and the signals of the thermocouple with a frequency of 2 kHz to cover the complete combustion process. The simultaneously Schlieren and OH* chemiluminescence imaging is performed with a frame rate of 20000 fps.
The high-speed Schlieren technique visualizes the evolution of hot jets and flame jets inside the main chamber. A modified z-type Schlieren setup with two parabolic mirrors and two smaller plane deflection mirrors are utilized to reduce the angle of rotation for the light beam and thus reduce the aberrations errors caused by the parabolic mirrors. A high power LED light source (Hardsoft Illuminator) generates visible red light in wavelength range of 610-660 nm with a luminous flux of 2100 lm to reduce cross-talk effects to the OH* chemiluminescence wavelength range. A Vision Research Phantom v1610 high-speed camera with a resolution of 896x800 pixels and an exposure time of 0.7 µs was used for the Schlieren image capturing. The spatial resolution is 16.0 pixels/mm. [22]
The determination of the heat release and the location of the flame front is possible by imaging of excited species such as OH* or CH* radicals. In this paper the OH* chemiluminescence imaging is used, due to its sharp band passed emittance near 307 nm and the clear separation from the broadband CO_2 signal. Under high pressure conditions the self-absorption characteristic of the OH (ground state) molecules, in the line of sight between the emitter and the detection optics, leads to a reduction in the light intensity of the OH* (exited) radical signal and requires the use of an image intensifier. The OH* intensity is interpreted as a marker for reaction and can be utilized as a useful diagnostic tool to indicate the location of the flame front and its propagation. Lauer &

Sattelmeyer [5] show that the integral chemiluminescence intensities can be correlated to the integral heat release, because the OH* creation is proportional to the CO_2 production inside the flame. [2, 3, 4]

A Vision Research Phantom v1610 along with a video-scope gated intensifier (LaVision high-speed IRO, cathode type: S20 P46) and a 105 mm UV lens were used to detect the exited OH* radicals. A narrow band pass UV-Filter (ASAHI Spectra ZBPA310) around 309±10 nm is used to separate the OH* signal. The image intensifier is synchronized with the high-speed cameras at an image frame rate of 20 kHz. The intensifier gate width is 10 µs and a lens aperture f5.6 was used for each experiment. To achieve the optimal intensity resolution the intensifier gain was adjusted at each shot. The comparability of each experiment with different intensifier gain settings is achieved by an image intensity normalization during the image post processing. The calibrated image intensifier sensitivity function is used for this purpose. The high speed camera operates with a resolution of 896x800 pixels corresponding to a spatial resolution of 10.7 pixels/mm.

2.2 Thermodynamic Post Processing

The first law of thermodynamics is applied to the transient pressure traces to calculate the heat release with a simplified approach in a constant volume vessel. It is assumed that the ratio of specific heats κ is constant. It is estimated as κ= 1.24 for an equivalence ratio of ϕ= 1 at the half temperature between the unburnt mixture temperature and the adiabatic flame temperature. The specific heat of the involved species is calculated by means of NIST (NASA) polynomials. The thermodynamic properties of the mixture are calculated under the assumption of perfect gas mixtures. The simplified heat release is estimated based on the approach of Hohenberg for internal combustion engines, known from [6]. The advantage of this procedure is the easy numeric calculation. Furthermore, the assumption includes an ideal gas and no wall heat losses. The discretized numerical solution for the heat release based on the energy conservation equation is [7]:

$$\left(\frac{dQ_H}{dt}\right)_i = \frac{1}{\kappa-1}\left\{\kappa \cdot p_i \cdot \left(\frac{dV}{dt}\right)_i + V_i \cdot \frac{p_{i+1}-p_{i-1}}{2\Delta t}\right\} \quad (1)$$

The term of a change in volume is set to zero in the investigated case of a constant volume combustion chamber. The integrated heat release is used to define and calculate burn durations and ignition delay times to characterize the velocity for different stages of the complete combustion process. The burnt mass fraction can be correlated to an ideally spherical expanding flame by the following equation:

$$\frac{V_{b\mathrm{burnt}}}{V_{\mathrm{total}}} = \frac{\mathrm{MFB}}{0.75\cdot\mathrm{MFB}+0.25} \quad (2)$$

The total chamber volume is 2186 cm^3 and for simplification it is assumed, that the trace of the normalized integrated heat release corresponds to the mass fraction burned profile. Figure 2.3 illustrates the correlation between the burnt to total volume ratio as a function of the burnt mass fraction. In comparison, the cylinder displacement

volume of typical gasoline engines on the market today usually is less than 500 cm^3 (which corresponds to 22.8% of the combustion bomb volume), while the combustion is already finished long before the piston has displaced this maximum volume. Aiming to understand the behavior of the PCSP combustion in a typical gasoline engine, obviously the focus of the analysis of the bomb combustion needs to be put onto the very early phase of flame progress.
The plot on the right in Figure 2.3 shows typical profiles for the integrated heat release (right axis) and the burnt volume ratio (left axis) for the standard spark plug ignition system and Pre-Chamber spark plug (PCSP). Again, for a proper comparison of the impact of the pre-chamber geometry on the combustion process inside the large combustion bomb in relation to a typical internal combustion engine with a cylinder volume of ~500 cm^3, it is necessary to analyze only the early points of heat release before 10% energy conversion. This heat release conversion time leads already to a slightly higher burnt volume than 500 cm^3 and will be defined as the late phase of combustion in regard to a typical engine combustion chamber. As can be seen from the Figure 2.3, the PCSP shortens the duration between ignition and the 20% energy conversion approximately by 35% compared to a conventional spark plug. The characterization of the early flame development phase will be based on the 2% and 5% energy conversion points. It could be shown, that the slope of the integrated heat release profile is sufficient to detect the 2% energy conversion point without any large numerical errors. On the other hand, a detection of 1% energy conversion timings gave instable and inaccurate results due to a too small gradient and will not be used in this work.

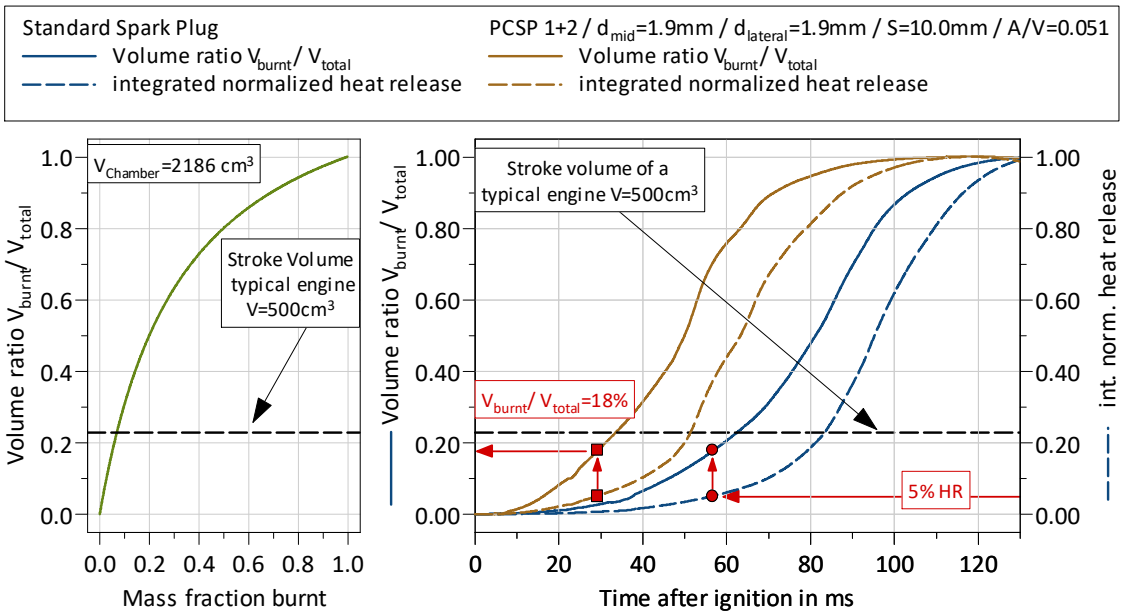

Figure 2.3: Comparison of heat release and burnt volume based on a spherical flame expansion

2.3 Image Post Processing

The Schlieren and OH* chemiluminescence images were acquired from two different perpendicular aspects with unequal spatial resolutions. One pair of lateral windows was used for Schlieren imaging and another perpendicular window provided the optical access for the OH* chemiluminescence image recordings. The comparability of the two imaging strategies necessitates several image post-processing strategies. Calibration measurements performed prior to the image recordings at the location of the spark plug perpendicular to the camera axis. Based on the calibration results the image aberration error is corrected as well the spatial resolution is determined. The following image processing is performed with MATLAB. First the OH* chemiluminescence image is scaled and offset corrected to the Schlieren image to enable a geometric comparison. In a second step an averaged background picture (10 images before the spark event are averaged) prior to ignition was subtracted from all images. The OH* chemiluminescence pictures were recorded with different intensifier gain settings to achieve a high signal-to-noise ratio. These pictures need to be corrected by normalizing it intensity to the minimum of the used intensifier gain during the complete campaign. The calibrated sensitivity function of the image intensifier is used for this purpose. The results enable a comparison of the OH* radical light intensity for different Pre-Chamber layouts and thus would allow a conclusion about the intensity of the early phase of combustion as well as on the ignition mechanism: flame jet or hot turbulent jet inside the main chamber.

2.3.1 Morphological Image Analysis

A morphological analysis of the Schlieren und OH* chemiluminescence images is the prerequisite for generating quantitative results of flame propagation and penetration depth of the turbulent jets.
The morphological reconstruction of the flame front and the burned area of luminous flames is widely discussed in the literature, e.g. [8-21].
There are several evaluated approaches available to detect the flame front, respectively the burned area, depending on the imaging type methodology selected. [11-13] use a combination of Otsu's binarization method and a user calibrated threshold to divide the picture into a burned and unburned area. The major drawback of this approach is that two calibration constants have to be estimated by the user. In addition, this method was developed to binarize images of a full spectrum luminous flame. The Otsu's threshold algorithm, a histogram-based approach, divides the pixels into two classes, so that the intra-class variance is minimized and the inter-class variance is maximized. The resulting threshold is used to binarize the image. This methodology needs images with a high contrast and a big signal-to-noise ratio. For this purpose the background-corrected images are filtered with a two-dimensional Gaussian kernel with a standard deviation of σ= 2.5 to reduce the fixed pattern and shot noise of the camera and the image intensifier. In a next step, the Otsu's binarization method with three threshold levels is applied. It was found that the use of two different thresholds improves the accuracy during the early flame evolution for the turbulent jets in contrast to the use of a single threshold value with OH* chemiluminescence signals. The upper two threshold levels can be considered as the burned gas area. The remaining noise and false pixel matches are removed by 7x7 pixels median filter. The count of burnt

pixels is the basis for the flame area and flame speed calculation. The Gaussian Filtering method was compared with a median filtering (filter size 7x7 pixels) prior to the Otsu binarization (see Figure 2.2 and 2.3). It was found that the latter method leads to monotonic increasing flame areas with reduced signal noise, when the burnt pixels from the previous time step remains unchanged in the current time step. The method using the Gaussian filtering causes unphysical normalized flame areas much smaller than unity in some cases, due to a high signal-to-noise ratio in the images. For these reasons the adapted Otsu binarization method with a median filtering will be used within this work (see Figure 2.2 and 2.3).

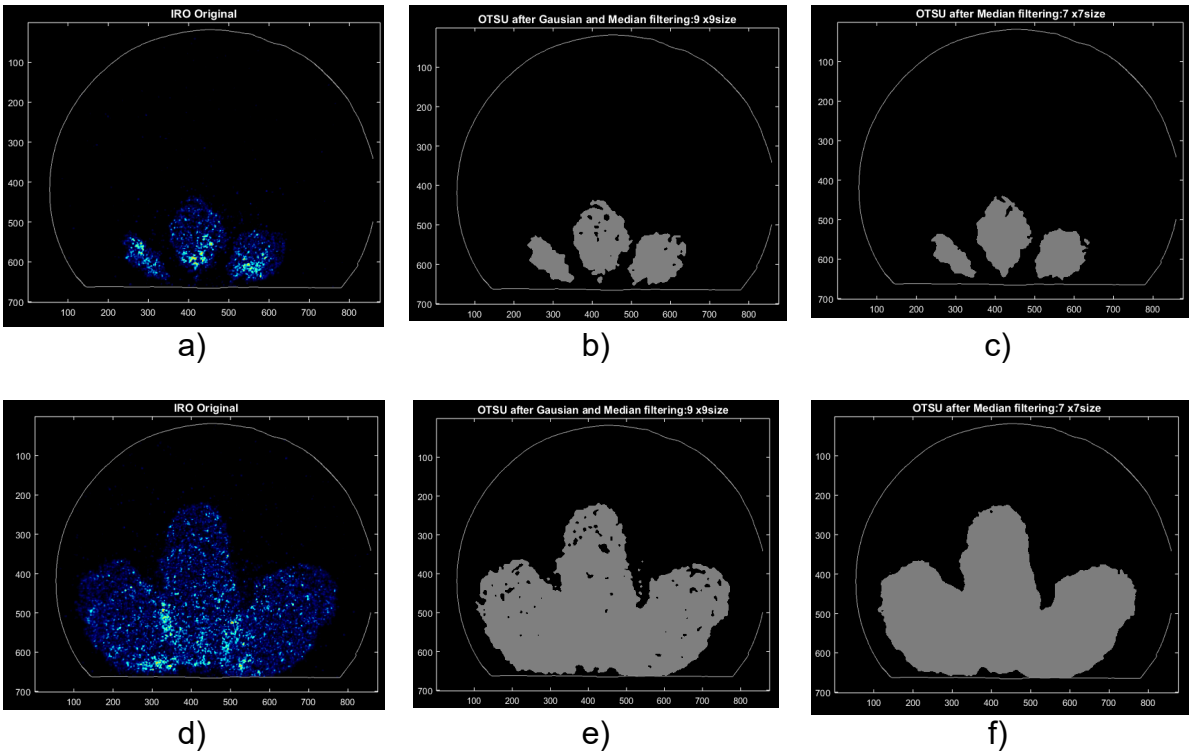

Figure 2.2: Comparison of image processing method (Gaussian filtering b-c, Median filtering e-f) prior to Otsu threshold for different timings with the original OH chemiluminescence images (a,d)*

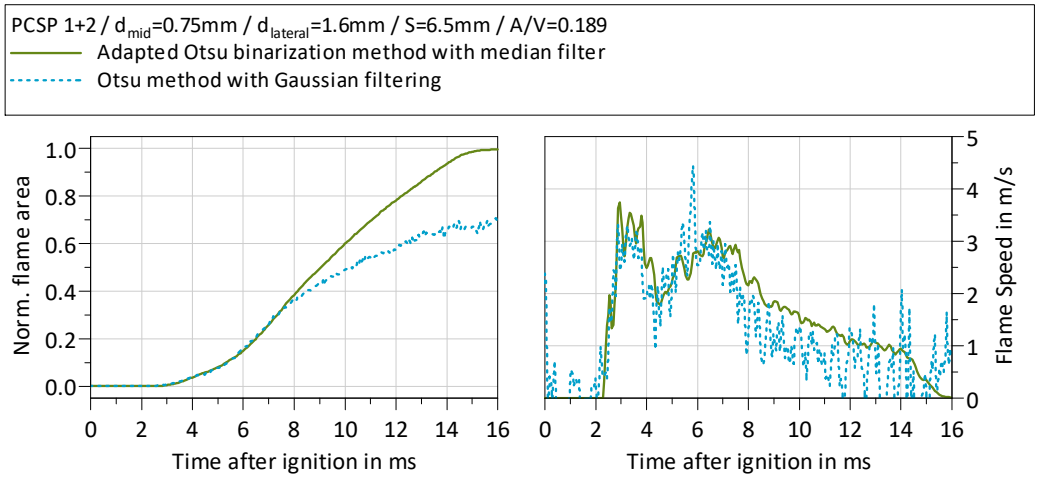

Figure 2.3: Comparison of normalized flame speed and flame area calculation for the mentioned different morphological image binarization algorithm

The penetration depth of the turbulent jets is estimated by using a different morphological image processing algorithm applied to the Schlieren pictures. After the ignition in the Pre-Chamber, hot gas jets penetrate into the main chamber through the overflow channels connecting the two chambers. For the analysis of different Pre-Chamber geometries it is important to estimate the jet penetration, as it provides information about gas and flame propagation, which is indirectly related to engine phenomena like inflammation reliability, knock tendency and burn duration.

a) Original image *b) Processed image*

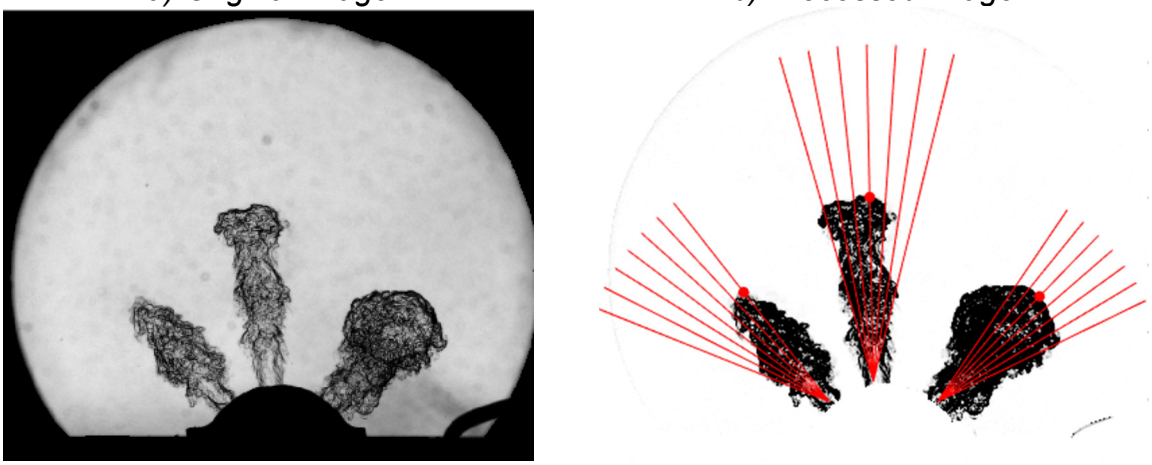

Figure 2.3: Determination of jet tip penetration inside the combustion chamber

The jet tip penetration is determined based on the Schlieren images inside the main chamber (see Figure. 3a). The background noise caused by camera CMOS chip is removed by a simple threshold method. In a second step, the recent Schlieren image is divided by the first image and normalized to enhance the contrast of the jet's front and to remove any dirt from the pictures. A quick and effective way to determine the jet penetration, is to evaluate the intensity of the pixels along a line orientated in jet direction. Since the jet can deviate when entering the main chamber, several lines with different angle but same origin (overflow-channel) are drawn, creating an array of lines (see Figure. 2.3b). The resolution can be changed by modifying the number of lines and the angle of the array. The maximal penetration is calculated for each line of the array and only the line with the highest penetration is retained. The position is tagged with a dot on the corresponding line in Figure 2.3b. This penetration is determined for each jet at each time step and exported to a data file.

3 Results

The development of well-adapted Pre-Chamber ignition systems requires the detailed technical understanding of the impact of Pre-Chamber geometry parameters to the basic mechanisms of fuel-air mixture inflammation and early flame propagation in the main combustion chamber under different thermodynamic boundary conditions. In order to examine the impacts without side effects, such as residual exhaust gas and charge motion, IAV has conducted a parameter study on a high-pressure combustion vessel. Limited by the mechanical durability of the chamber and the available power of the electrical heating device, the combustion cell enables the adjustment of chamber conditions at ignition timing of up to 18 bar and 398 K. Especially high load and catalyst heating operating points differ quite significantly from these conditions under real engine operation.
Nevertheless, it was tried to define operating points for the combustion vessel with best relevance for real engine operation. A simple approach for the comparability of boundary conditions is the correlation of the unburned gas density. The lower temperature inside the combustion bomb would be compensated by corresponding lower pressures in order to match the gas density. However, pressure and temperature do also have a significant impact to the laminar flame speed of the mixture.

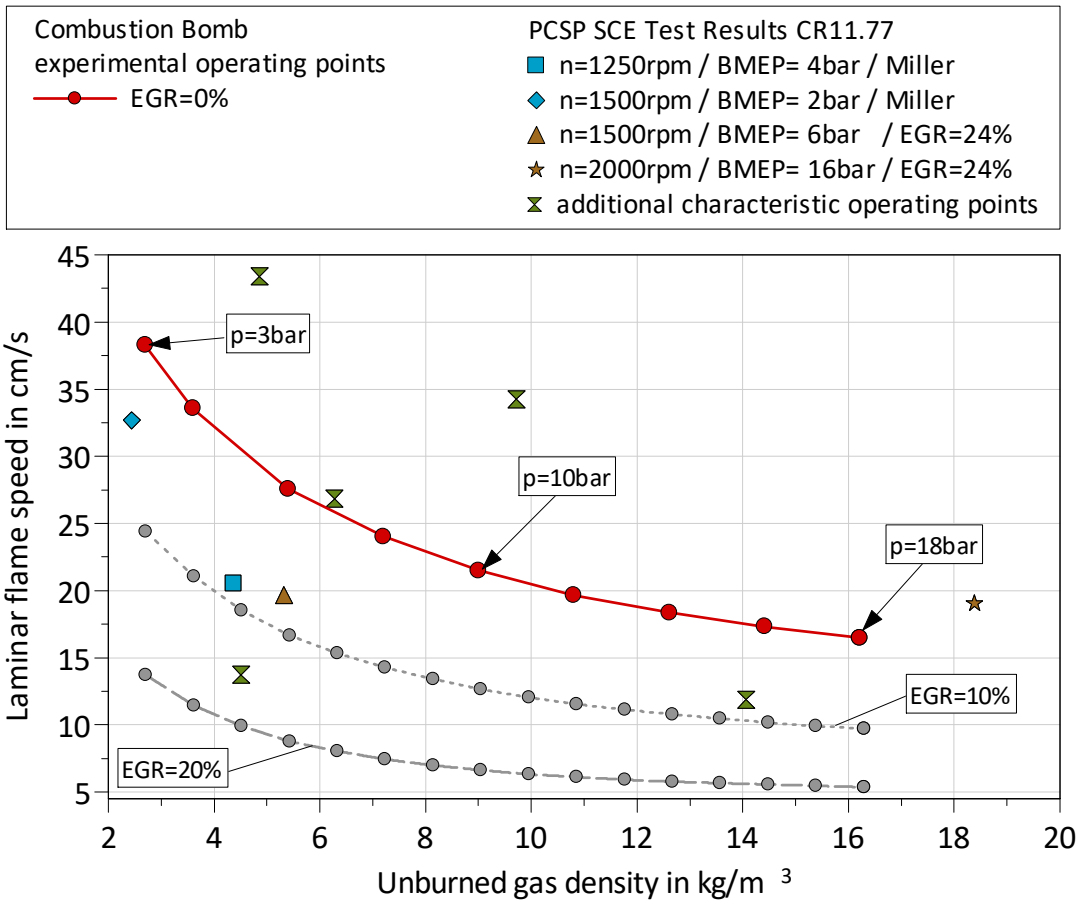

Figure 3.1: Laminar flame speed for a stoichiometric methane air mixture for different pressures and unburned gas temperatures inside the high pressure combustion cell. Comparison with typical engine operating points in consideration of its specific thermodynamic properties (temperature, pressure and residual gas rate)

A main scope of this work is the visualization and analysis of the flame / hot gas jets passing over from the Pre-Chamber to the main chamber (after the initial ignition inside the Pre-Chamber) as well as the early flame propagation inside the main chamber. From this perspective, the laminar flame speed is considered the most important parameter for the correlation of the operating points of combustion vessel and single cylinder engine. Figure 3.1 illustrates the laminar flame speed for a stoichiometric methane air mixture for different pressures and unburned gas temperatures inside the high pressure combustion bomb in comparison to different characteristic engine operating points – considering the specific thermodynamic and chemical properties (gas composition, temperature and pressure). The calculations have been conducted with the chemistry solver of CONVERGE by Convergent Science based on the GRI3.0 reaction mechanism with 53 species [23].
Referring to these preliminary considerations, three main operating points have been defined for a comprehensive parameter study in the combustion bomb – 3, 10 and 18 bar chamber pressure at ignition timing. These points can be set in relatively good correlation to characteristic single cylinder engine operating points – based on comparable laminar flame speed. 18 bar chamber pressure (at 398 K chamber temperature) represents in good approximation the medium high load operation of the single cylinder ICE (2000 rpm / 16 bar BMEP), 10 bar chamber pressure the part load map area (1500 rpm / 6 bar BMEP) and 3 bar chamber pressure the critical low load / catalyst heating operation (1250 rpm / 2 bar BEMP). In addition to those main operating points also other chamber pressures have been investigated with selected PCSP configurations.
Table 3.1 summarizes the experimental space of the geometric Pre-Chamber parameters and thermodynamic boundary conditions investigated inside the combustion vessel.

Table 3.1: Experimental space of geometric PCSP parameters and thermodynamic boundary conditions

Parameter	Unit	Range	Description
Number of bores	-	3 – 7	total
Bore layout	-	1+2 / 1+5 / 1+6	central + lateral
Central bore diameter	mm	1.0 – 3.5	
Lateral bore diameter	mm	1.0 – 1.9	
Spark location	mm	3.5 / 10 / 16.5	
PC Volume	cm³	1.27 / 1.65 / 2.02	spark location low / middle / high
A/V	-	0.012 – 0.173	bore area to PC volume ratio
Spark plug size	-	M10	mass production, 2 electrodes
Gas temperature	°C	115 – 128	
Gas pressure at ignition	bar	3 – 18	
Lambda	-	0.95 – 1.5	

Figure 3.2 shows examples of the investigated PCSP variants. The two right 1+2 bore designs have been defined in order to achieve best visualization of the Pre-Chamber jets without disturbing interferences of the single streamers within the experimental setup of the combustion bomb. Thus most investigations have been conducted with those bore layouts. The two left 1+5 and 1+6 bore designs were expected to create interferences of the different jets and thus to complicate the result analysis, however, have been tested in brief measurements in order to have the best possible overlap to the PCSP designs investigated inside the single cylinder engine.

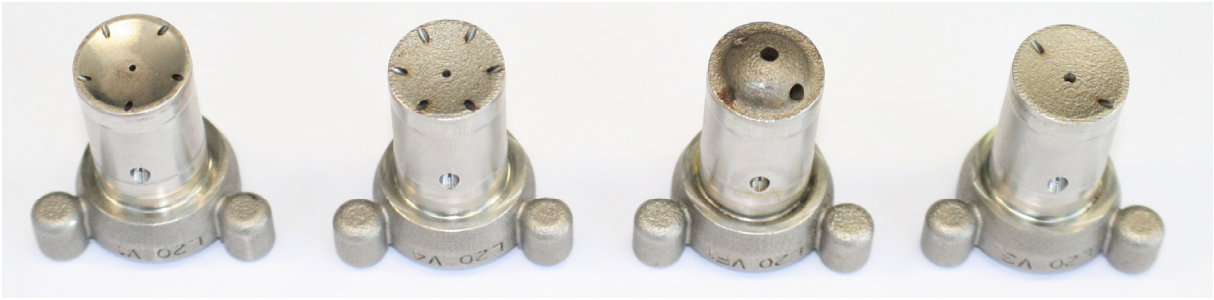

Figure 3.2: Examples of investigated PCSP variants

3.1 Measurement repeatability and mixture homogeneity

In order to validate the repeatability of the high-pressure cell investigations, a series of repeated measurements has been conducted at the beginning of the test campaign. Figure 3.3 shows the repeatability of 3 to 5 measurements for one exemplary Pre-Chamber configuration at three different equivalence ratios.

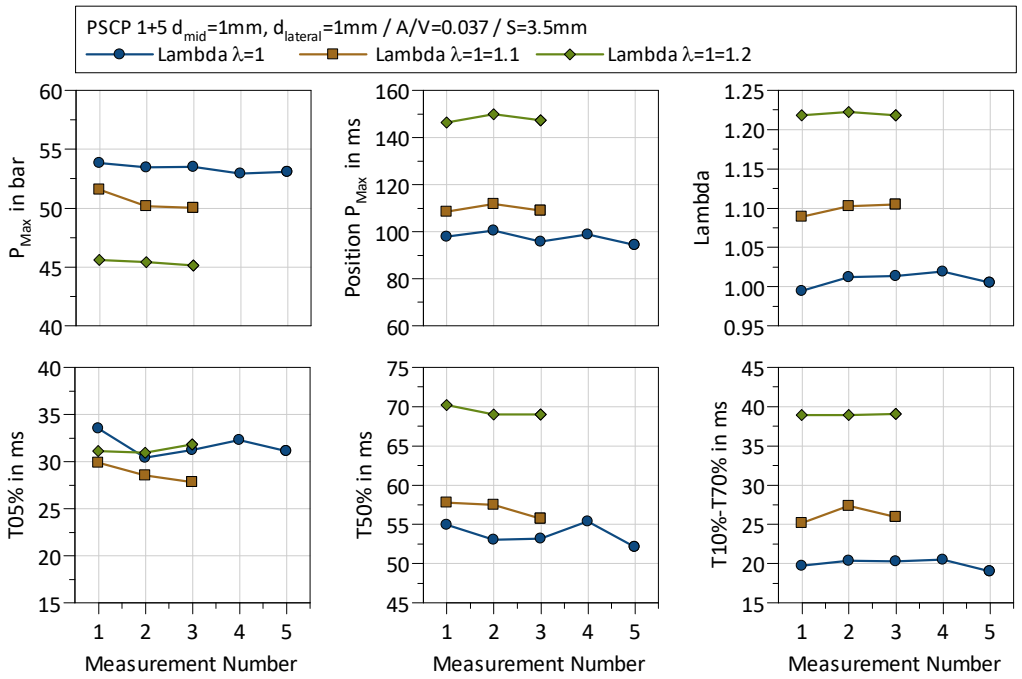

Figure 3.3: Evaluation of the measurement repeatability for one exemplarily Pre-Chamber spark plug with a spark location S=3.5mm for 10 bar ignition pressure and different equivalence-ratios.

Overall, there is a very good repeatability and thus validity of the measurement results. For the subsequent test campaign, each configuration has been measured twice. If the results have been within an acceptable deviation, they were averaged for further analysis. In case of bad repeatability, a third measurement has been conducted to identify measurement outliers. Figure 3.4 illustrates the flame front development of the standard spark plug ignition system at a system pressure of 3 bar. The flame front propagates spherical after the ignition process. This indicates a highly homogenous mixture in terms of equivalence-ratio and temperature distribution inside the combustion chamber and is in accordance to the laminar flame propagation theory inside a combustion chamber.

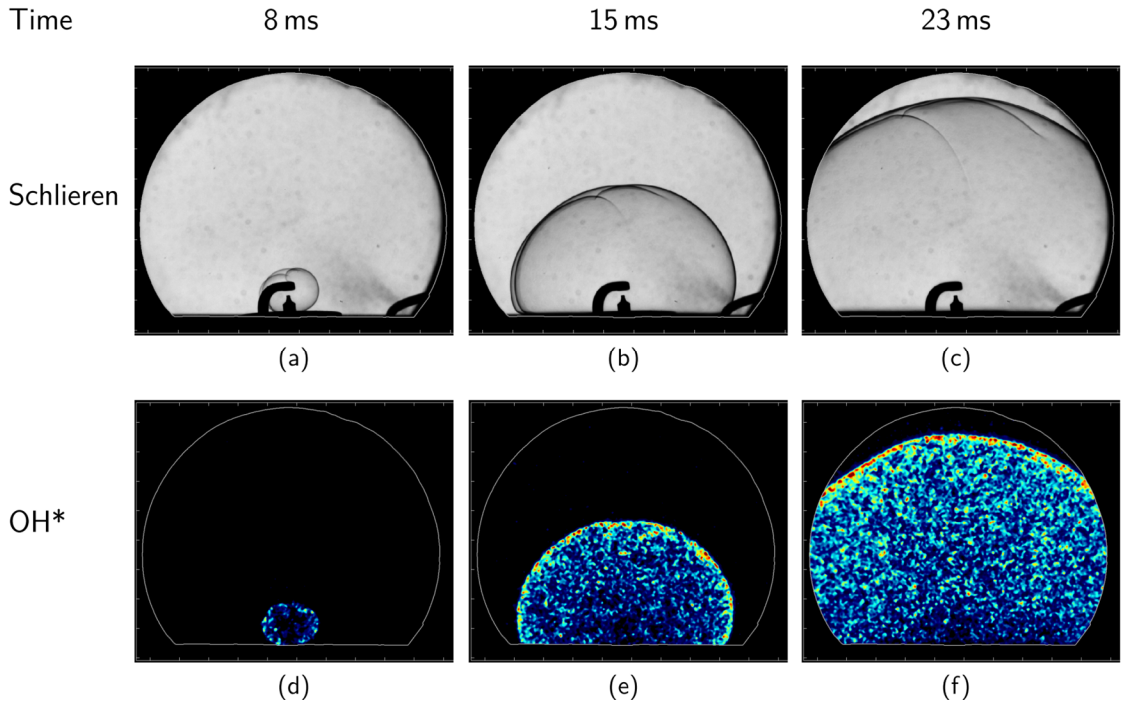

Figure 3.4: Evaluation of the flame front for the standard spark plug ignition system at 3 bar ignition pressure. Top Row: Schlieren images. Bottom Row: OH-Chemiluminescence images at different times. Ignition timing is at 5.5ms.*

3.2 Dependency of Pre-Chamber geometry and pressure on inflammation process in the main chamber

As known from previous single cylinder investigations [1, 24] the PCSP geometry might have a very positive impact on knock resistance, while the low load performance is quite challenging to improve to a level known from conventional ignition systems.
It was found, that a small A/V-ratio could have a very positive impact to knock mitigation. However, for low engine loads a different PCSP design with for example higher A/V-ratio and adapted bore layout is rather beneficial. Therefore an optimal Pre-Chamber spark plug design has to solve the trade-off between a high knock resistance and reliable inflammation at poor ignition conditions. Figure 3.5 illustrates the early heat release and the flame propagation as a function of the ignition pressure for three different PCSP geometries and the conventional spark plug ignition system. An increasing ignition pressure is achieved by a higher mixture mass and thus leads to the trivial result of an increasing maximum pressure of up 100 bar inside the main chamber. The mechanical durability of the combustion vessel limits the peak pressure to 100 bar.

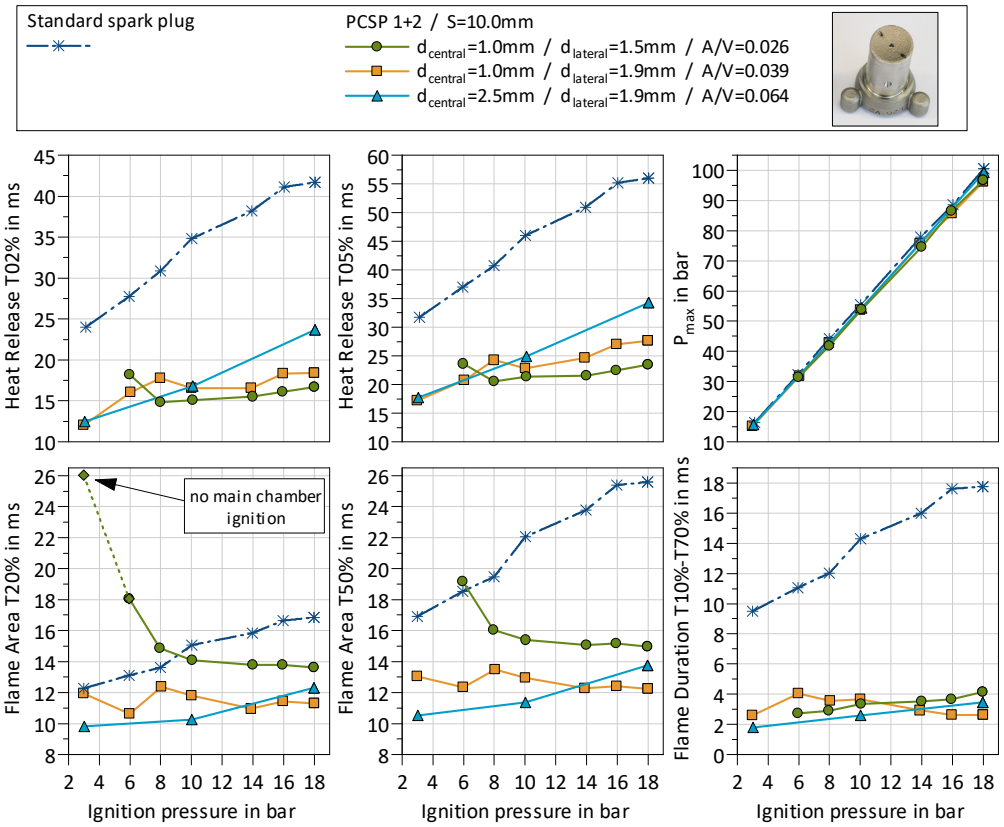

Figure 3.5: Effect of different central overflow channel diameter sizes on flame propagation and heat release for distinct ignition pressures. Equivalence-ratio ϕ=1.

A higher mixture mass as a consequence of an increased pressure results in a prolongation of the heat release. This is caused by a reduced laminar flame speed for higher pressure as shown in figure 3.1. The standard spark plug ignition system shows, as expected, the longest period of heat release. Schlieren images indicate a largely laminar flame expansion during the first phase of combustion. Later on cellular flame instabilities (Darrieus-Landau and thermo-diffusive instabilities, for more information refer to [7]) could be observed, which are a typical phenomenon of a spherically expanding flame in the case of the standard spark plug ignition system. These instabilities and

the curvature of the expanding flame increase the laminar flame velocity estimated by the image analysis process. That is comparable to the physical phenomenon of a turbulent flame propagation. The calculated flame speed for the standard spark plug ignition system is overestimated in these cases. The image analysis procedure also assumes that the flame area is equal to a circle. The flame speed calculation is based on the temporal derivation of the circle radius and thus leads to several inaccuracies for the absolute flame speed values, because the three dimensional flame surface is projected to a two dimensional image recorded by the camera. As well, the flame formation for the PCSP has a completely different shape compared to a circle. Nevertheless this methodology allows a quantitative comparison within the measurement campaign between the conventional spark plug ignition system and different Pre-Chamber geometries.

The standard spark plug shows a significantly increasing flame duration (Flame duration T10%-T70%) for an elevated ignition pressure. The dependency for the PCSP variants is nearly one order of magnitude smaller than for the spark plug. The Pre-Chamber with an A/V-ratio of 0.064 and a central bore diameter of 2.5 mm shows a similar behavior to the conventional ignition system. It can be stated that a large bore diameter is beneficial for low load conditions and disadvantageous at high ignition pressures for achieving reliable inflammation and short inflammation delays. A very small central bore diameter in combination with a small A/V-ratio of 0.026 prevents an inflammation at 3 bar and leads to a significant prolongation of the inflammation delay (Flame Area T20%) and the early heat release. The smaller bore diameter increases the jet mean velocity, the fluctuation speed and reduces the characteristic size of the turbulent eddies. For a stoichiometric methane mixture at 3 bar, the laminar flame thickness is in the order of 0.25mm. For an orifice diameter of d=1.0mm it can be assumed, that the tiniest turbulent eddies are smaller than the flame thickness and can therefore rip the flame front inside the overflow channel. Furthermore the highly turbulent jets lead to a rapid mixing and thus an increased heat loss to the preheat zone. The flame extinguishes and avoids a stable inflammation at low pressure and temperature conditions. A higher ignition pressure increases the mixture mass inside the Pre-Chamber. The heat release is intensified and the laminar flame thickness is reduced to approx. 0.07 mm. This leads to a reduced flame quenching probability for higher ignition pressures. The flame ignition mechanism becomes more prevalent [7, 27, 32].

Figure 3.6 illustrates the jet structure and the OH* intensity for the above mentioned Pre-Chamber geometries at three characteristic ignition pressures. The investigated PCSP variants show increasing density gradients for elevated pressures. This characteristic can be explained by the higher mass burnt inside the Pre-Chamber, which leads to an intensified energy input into the main chamber. In general it can be stated, that the inflammation is always induced by the bore with the largest diameter. The highest OH* intensities are observed for the PCSP with A/V ratio of 0.039, which seems to be in the optimal range for a reliable inflammation at low and high loads. The structure of the central jet changes from a typical open jet characteristic to mushroom-shaped jets for a bore diameter of 2.5 mm.

Overall, it can be claimed, that there is an optimal cross section area to volume ratio with a least one larger bore diameter, to enable a reliable inflammation at low loads and only a minor flame speed prolongation for higher ignition pressures. If the A/V-ratio becomes too small, the inflammation delay (flame area T20%) and the early flame formation period (flame area T50%) increase, especially for high loads.

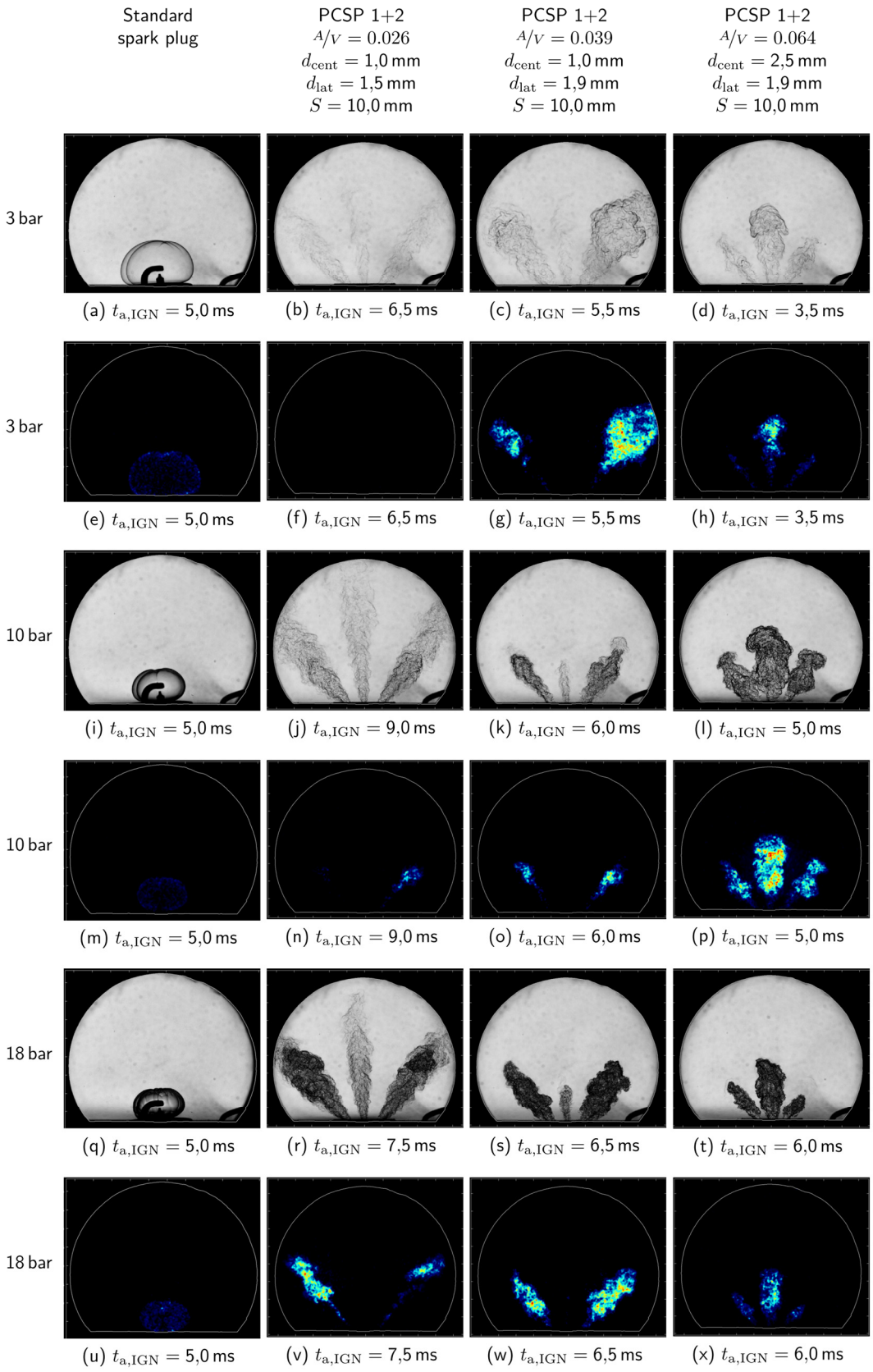

Figure 3.6: Effect of different central overflow channel diameter sizes on the flame jet structure and the OH intensity. Ignition pressure p=3 bar. Equivalence-ratio ϕ=1.*

3.3 Dependency of Pre-Chamber geometry on the flame formation under low pressure and low temperature conditions

In [1] and [24] it was found at a single cylinder research engine, that low load and low temperature conditions cause small pressure differences between the Pre-Chamber and the main chamber and thus resulting in low jet velocities. Consequently, this weak jet is rather unlikely to ignite the mixture in the main combustion chamber. Based on these previous findings it might be reasonable to assume that low wall temperatures and small overflow channel diameters increase the resistance for the flame to propagate from the Pre-Chamber into the main chamber. The strong and highly turbulent flow field inside the bores leads to an intensive flame stretching and in addition with a large surface contact area to the colder walls to an in tendency increasing flame quenching. In [24] it was stated, that a PCSP with an increased cross section to volume ratio in combination with a larger central bore diameter enhances the ignitibility and combustion stability at a typical catalyst heating operating point.

Figure 3.7 illustrates the impact of the overflow channel cross section area to the Pre-Chamber volume (A/V) with identical spark locations at an ignition pressure of 3 bar. The pressure difference between the Pre-Chamber and the main combustion chamber increases for smaller A/V-ratios, due to a higher flow resistance of the overflow channels. Comparing the excess pressure for the different geometric PCSP layouts with the tiniest A/V-ratio, it can be expected, that there is an A/V-ratio lower limit for a proper ignition of the mixture inside the main chamber. The PCSP layout with the smallest A/V-ratio and only three overflow channels generates overly weak flame jets with only marginal OH* luminescence detected, which in turn could not ignite the main mixture inside the combustion bomb. The 1+5 PCSP layout with smaller bore diameters does not show any OH* radical concentration at all (see Figure 3.8). This fact is a strong indicator, that the flame extinction is mainly induced by the too small bore diameter. The heat transfer from the reacting fluid to the cold walls, the strong flow field inside the overflow channels and the flame stretching are assumed to be the main causes for this characteristic at low loads. Increasing the A/V ratio leads to a reduction of the period for flame formation and thus to faster heat release in the early stage of combustion prior to an energy conversion up to 10%.

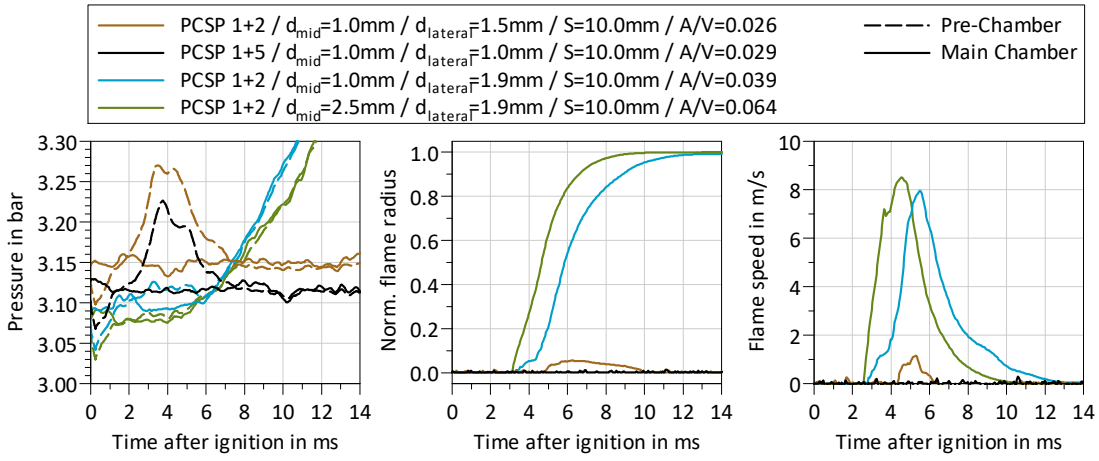

Figure 3.7: Impact of the overflow channel cross section area on the flammability of the main chamber mixture. Ignition pressure 3 bar and equivalence-ratio ϕ=1.

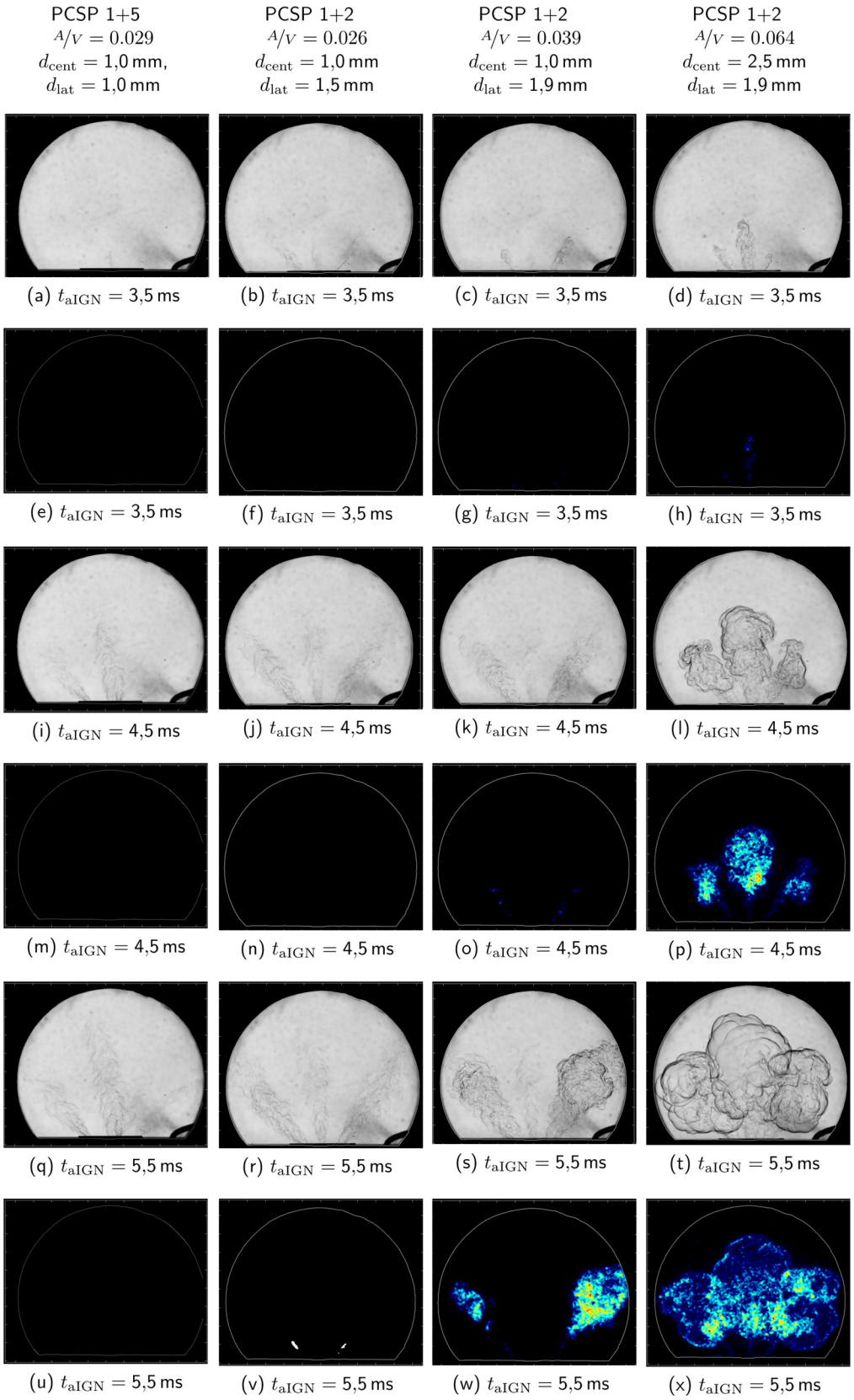

Figure 3.8: Impact of the overflow channel cross section area on flame propagation for different PCSP configurations visualized by Schlieren and OH intensity images ((v) shows binarized flame image for a better visualization, due to very weak intensity). Ignition pressure p=3 bar. Equivalence-ratio ϕ=1.*

Figure 3.8 illustrates the jet penetration (Schlieren images) and the OH* chemiluminescence intensity for the mentioned PCSP configurations at different timings after ignition. The 1+5 PCSP with A/V=0.029 shows weak non reacting hot jets entering the main chamber. The 1+2 PCSP with the smallest A/V=0.026 with a lateral bore diameter $d_{lateral}$=1.5 mm shows weak lateral flame jets exiting the Pre-Chamber 6.5 ms after the ignition. This indicates that the bore diameter is the major factor for the flame quenching during the overflow process of the flame from the PC to the main chamber. It can be assumed that the larger diameter of the lateral bores avoids an extreme flame wrinkling and thus prevents the flame from quenching inside the overflow channels compared to the smaller central bore with a diameter of $d_{central}$=1.0 mm. The ignition energy of the lateral flame jets is too small to ignite the main chamber mixture. The third PCSP configuration is achieved by an enlargement of the lateral bore diameter to $d_{lateral}$=1.9 mm. The ignition occurs in the core area of the lateral jets. After the inflammation of the main chamber mixture, the flame propagation is mainly driven by the motion of the turbulent shear layer of the jet. The last PCSP configuration with a central bore diameter of 2.5 mm and lateral bore diameters of 1.9 mm supports the thesis, that the flame is first transported by the potential core of the hot jet exiting the overflow channel with largest cross section area. The lateral overflow channels leads to additional retarded ignition sources with smaller OH* intensity. If the ignition delay is defined as the appearance of the first OH* radicals inside the main chamber, then a higher A/V-ratio shortens the ignition delay. In contrast, the robust inflammation by a flame jet is directly dependent on the overflow channel diameter and thus only indirectly influenced by the A/V-ratio for low load and temperature conditions.

Figure 3.9 shows the impact of the PCSP geometry, the spark location and the A/V-ratio on characteristic energy conversion timings and the relative visible area covered by the flame. The two PCSP geometry variants differ in the size of the central and lateral bore diameters and in the structure of the shape towards the main chamber. The PCSP variant with a convex shape is termed as Thimble. The PCSP leads in general to a faster energy conversion compared to the standard spark plug ignition system. The early detection of the 20% flame area for the conventional spark could be explained by a fast grow of the initial flame kernel inside the main chamber. In case of the PCSP configurations the initial flame kernel is generated inside the exterior Pre-Chamber volume and thus leads to minor or no advantages in terms of the early flame propagation inside the main chamber. As explained above, it could be found a lower limit of the A/V-ratio in the range of 0.021 to 0.026, which limits the ignition probability inside the main chamber. An elevated spark location S=16.4 mm can extend the lower limit. The larger Pre-Chamber volume with a higher mixture mass increases the energy release and therefore the energy input of the hot jets into the main chamber gases. The convex Thimble Pre-Chamber designs show in general advantages for the speed of heat release and flame development. The only explanation for such a characteristic is the different coverage angle between the central and the lateral jets. The central and lateral jets enables a faster flame expansion, because there is a delayed interaction of the flame front from the three jets. The jet interferences occur later for Thimble PCSP configurations and decelerate the combustion process.
The lower spark location S=3.5 mm and an increasing A/V-ratio lead to a deceleration of the combustion and early flame expansion speed. The larger the cross section area, the more the flame propagation characteristic become similar to the performance of a conventional spark plug. The intermediate spark location S=10.0 mm results in the fastest heat release and flame duration T10%-T70%. The biggest advantage in energy

conversion is achieved with an intermediate cross section to Pre-Chamber volume ratio in the range of 0.04 to 0.052. The convex PCSP with a high spark location S=16.4 mm shows a minor temporal benefit for the 10% of energy conversion. This indicates, that a larger Pre-Chamber volume generates more reactive and turbulent jets. The more turbulent flow field and reaction energy sustain the highly turbulent combustion character for a longer period and thus improve the combustion speed in large cylinder volumes.

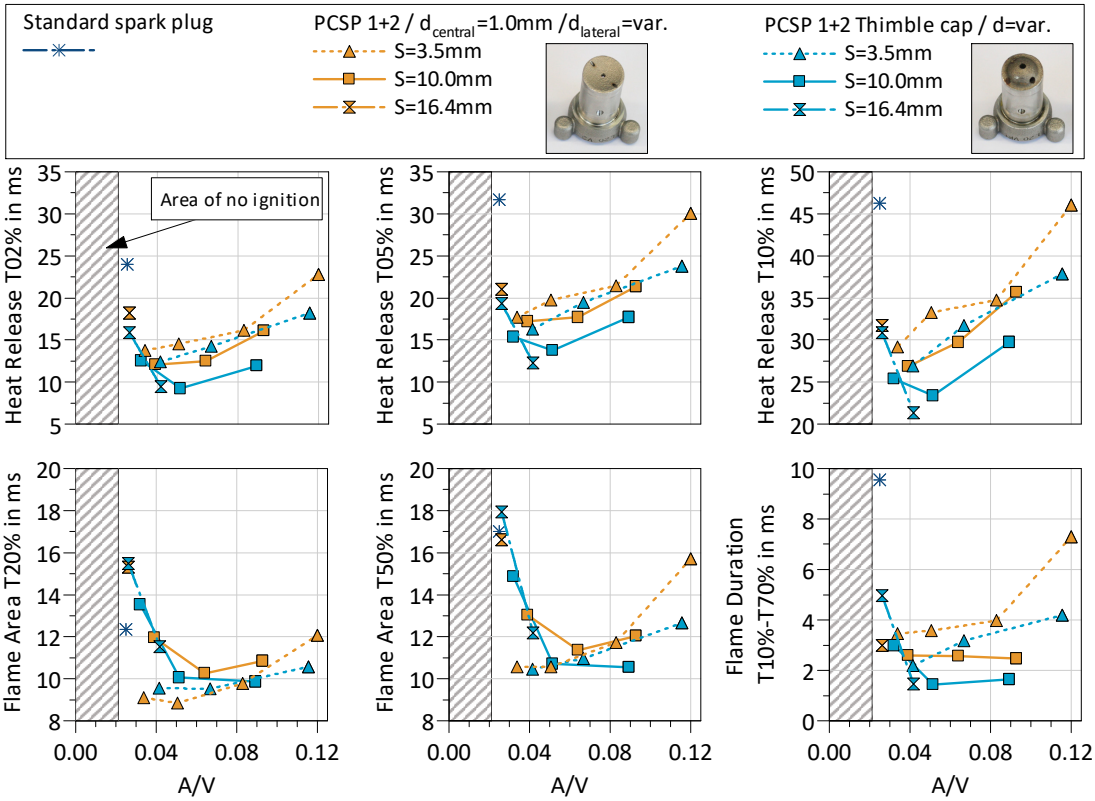

Figure 3.9: Impact of the overflow channel cross section area and spark location on the thermodynamic heat release and the flame propagation for different PCSP configurations in comparison to the standard spark plug ignition system. Ignition pressure p=3 bar. Equivalence-ratio ϕ=1

Figure 3.10 compares the jet penetration and the inflammation process for three different Pre-Chamber layouts with the standard spark plug ignition system. The 1+6 PCSP (right) is a more typical ICE design, that is used to create multiple spatial distributed ignition sources in order to enable a short burn duration and to capture a large volume in the vicinity of the combustion chamber roof. The PCSP layout with an identical A/V-ratio but a different number of overflow channels (1+2 vs. 1+6) and larger bore diameters (1.9 mm vs. 1.25 mm) shows a significant reduction of the inflammation delay in the main chamber after ignition onset in the Pre-Chamber. The 1+2 PCSP layout with a smaller A/V-ratio of 0.032 (bore diameter 1.5 mm vs. 1.9 mm) leads to a comparable inflammation delay to the Pre-Chamber with seven holes. This suggests that the bore diameter is the relevant parameter for a short ignition delay and a robust inflammation inside the main chamber.

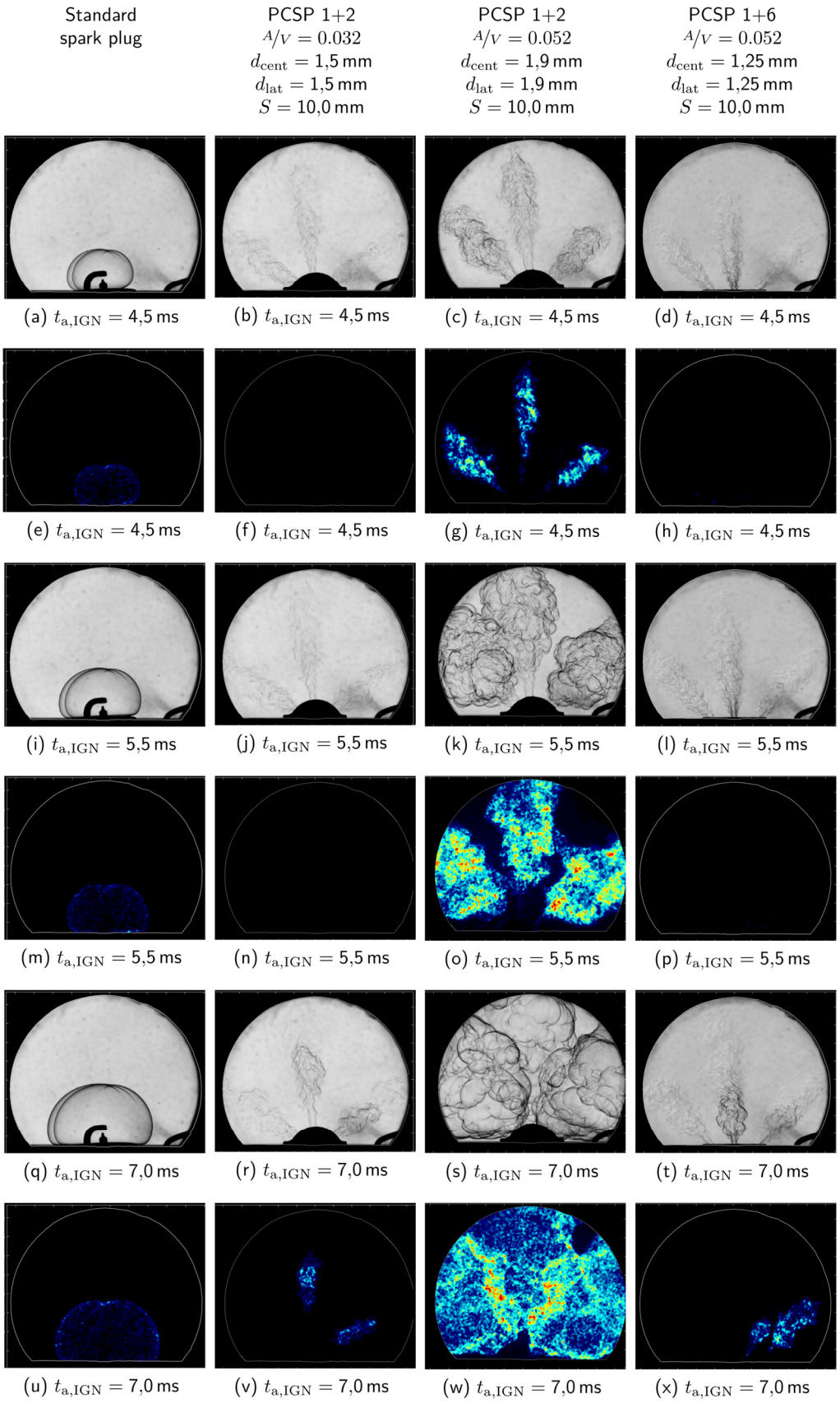

Figure 3.10: Impact of the overflow channel diameter on flame propagation for different PCSP configurations visualized by Schlieren and OH intensity images. Ignition pressure p=3 bar. Equivalence-ratio ϕ=1. Spark location S=10.0 mm.*

The inflammation inside the main chamber for the 1+6 PCSP design and the 1+2 layout with an orifice diameter of 1.5 mm occurs only at two jets. Without an optical access to the flame propagation inside the Pre-Chamber, shaped like a pipe with small openings, it can just be assumed that the flame formation inside the cylindrical Pre-Chamber is comparable to a tulip flame. A tulip shaped flame front can often be observed in closed or half-open ducts. The evolution of such a shape can be described by the following phases. At first the flame kernel expands spherical with the laminar flame velocity until the flame front reaches the side walls. The wall contact leads to rapid reduction of the flame surface area and a deceleration of the propagation speed. When the flame extinguishes near the walls, the curvature of the flame front is inverted, because the unburnt gases are reflected into the middle of the tube. Depending of the tube geometric sizes (diameter, length, cross section area of the opening) the flame front near the centerline can move backwards. In some cases there were observed oscillating propagations of the tulip flame that causes pressure oscillations. Considering the inflammation preferred to individual jets, it is an indication for a distorted tulip shape flame formation inside the Pre-Chamber. For a better understanding of the inflammation process in the main chamber, it is necessary to investigate the flame evolution with optical methods inside the small Pre-Chamber volume. [28, 29, 30]
Figure 3.11 shows the pressure difference between the Pre-Chamber and the main chamber, the flame radius and the jet penetration depth for these PCSP configurations. The Pre-Chamber variants with an identical geometric A/V-ratio causes a comparable pressure rise inside the Pre-Chamber, but leads to a complete different flame formation and penetration of the central jet. It can be assumed, that the pressure difference between the Pre-Chamber is mainly a function of the geometric A/V-ratio and independent of the number and the diameter of orifices.

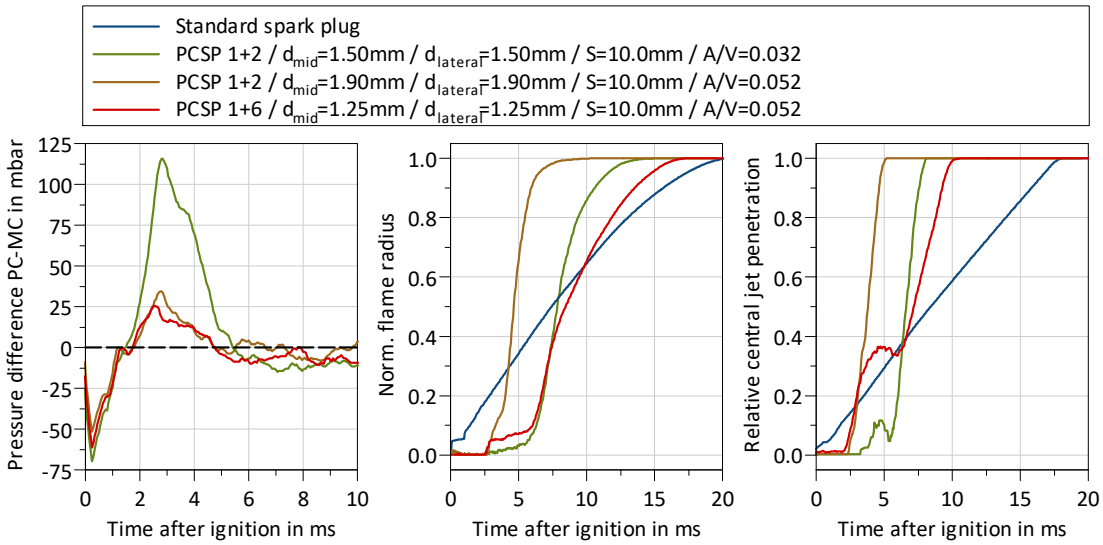

Figure 3.11: Impact of A/V-ratio on pressure rise in the Pre-Chamber, flame radius and the jet penetration. Ignition pressure p=3 bar. Equivalence-ratio ϕ=1. Spark location S=10.0 mm.

Figure 3.12 and Figure 3.13 illustrate the impact of the central orifice diameter on the inflammation and the jet penetration into the main chamber for a spark location S=10.0 mm. The first flame occurs in general at the orifice with the largest diameter. The shortest inflammation delay in combination with the highest OH* intensity is achieved by an intermediate geometric A/V-ratio. A further increase of that geometric parameter leads to a deceleration of the inflammation process. The increase of the central bore diameter reduces the flow restriction between the Pre-Chamber and main chamber. As discussed above, the pressure rise decreases and induces a reduction of the flow velocity in the overflow channels. Consequently the turbulence intensity decreases and the characteristic turbulence length scale becomes larger. The Schlieren images illustrate, that the shape of the middle jet changes significantly for an orifice diameter larger than 2 mm from a characteristic open jet shape to a mushroom-shaped flow structure. This mushroom-shaped structure grows much faster perpendicular to the jet longitudinal axis and thus enables a faster capture of the unburnt gases. A closer look at the PCSP configuration with a central orifice diameter of 2.5 mm suggests, that a specific diameter ratio among the large and the smaller orifices leads to the fastest flame area evolution under poor ignition conditions.
Figure 3.12 supports this hypothesis, showing that a central orifice diameter of 2.5 mm achieves the fastest jet penetration and the shortest flame evolution period. The first temporal rise inside the Pre-Chamber characterizes the early inflammation phase in the visible spatial range of the observation windows and correlates well with onset of the first flame inside the main chamber. The higher the pressure rise, the later the beginning of the flame formation.
The steep gradient in the pressure difference occurs first on the Pre-Chamber pressure transducer signal. It may be expected, that this behavior is induced by the strong temperature rise in the Pre-Chamber caused by the gas ionization after the ignition. The pressure transducer is located only a few millimeters away from the spark plug. This signal trace is typical for a thermal shock of a pressure transducer. [31]

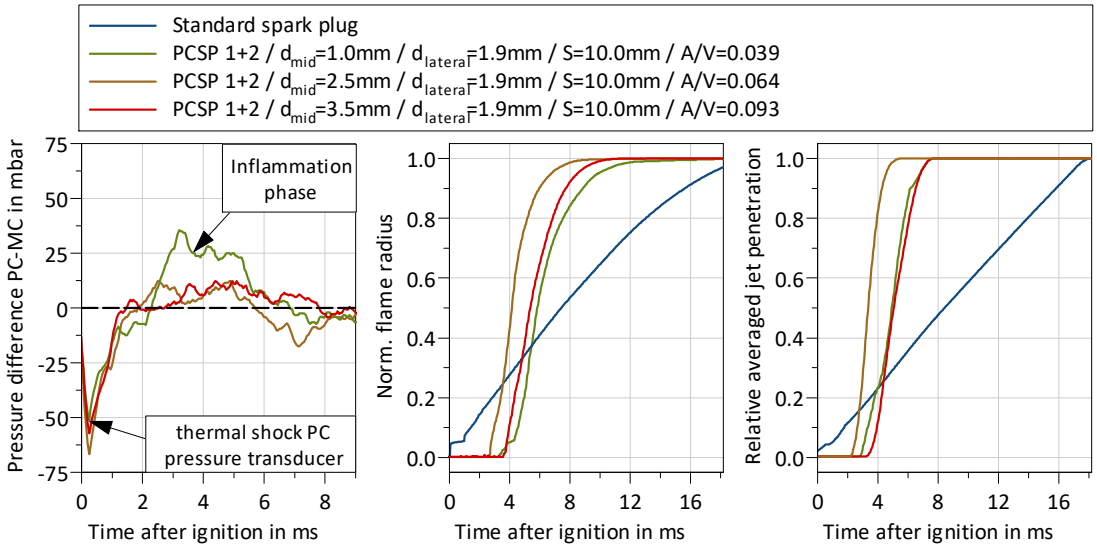

Figure 3.12: Impact of the central orifice diameter on flame evolution, averaged penetration of the three jets and pressure rise inside the Pre-Chamber. Ignition pressure p=3 bar. Equivalence-ratio ϕ=1. Spark location S=10.0 mm.

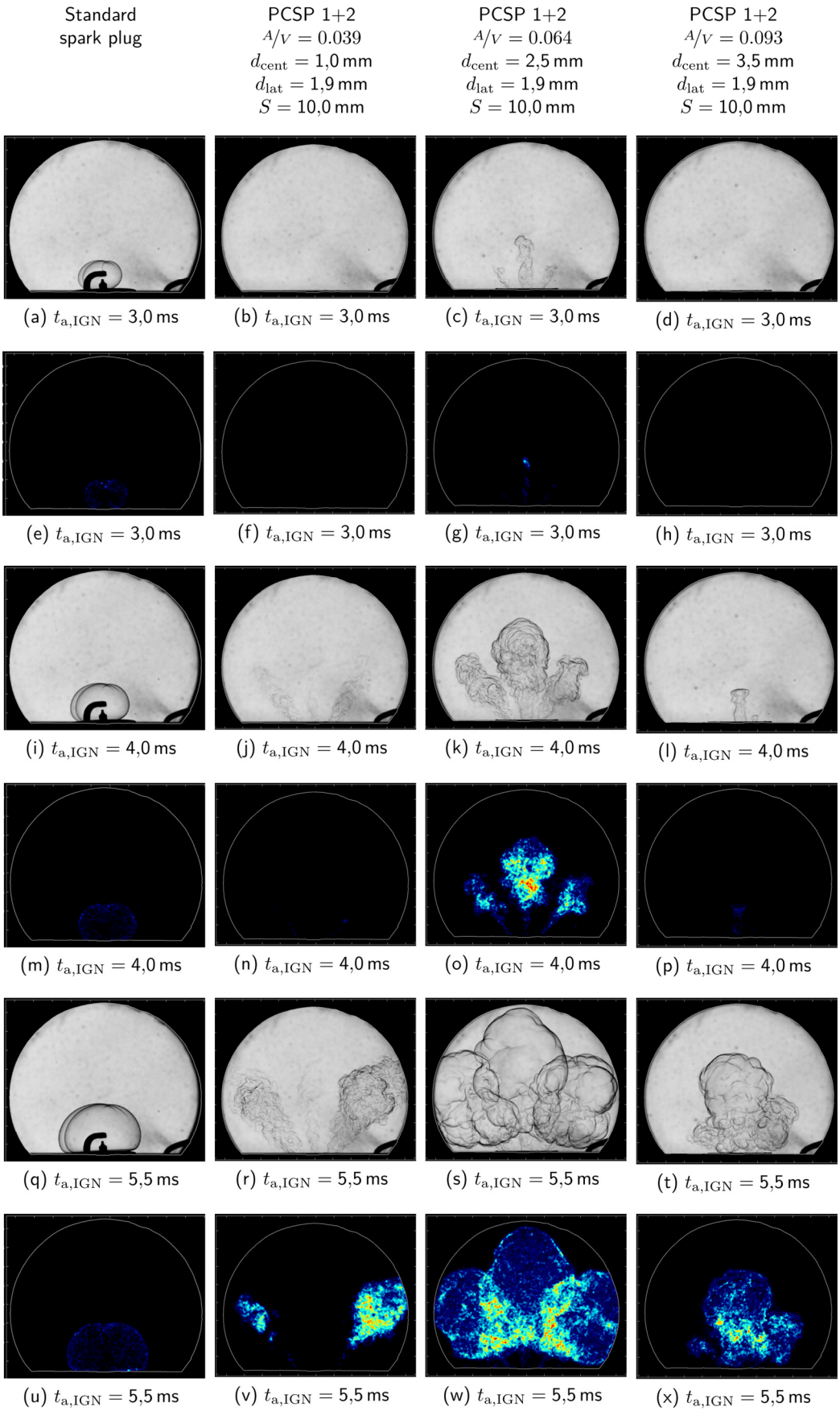

Figure 3.13: Impact of the central bore diameter on flame propagation and jet structure. Ignition pressure p=3 bar. Equivalence-ratio ϕ=1. Spark location S=10.0 mm.

3.4 Dependency of Pre-Chamber geometry on the flame formation under high pressure conditions

In [1] and [24] was found that a PCSP ignition system has a noticeable potential for knock mitigation. The characteristic is caused by the creation of multiple spatial ignition sources, a high turbulence production through the flame jets and thus a reduced burn duration. As mentioned in chapter 1.2, the potential is dependent on the geometric layout, the material and the system integration. This section discusses the impact of the geometric layout of the Pre-Chamber on the inflammation and early heat release under high pressure conditions. An engine load of 16 bar BMEP at an engine speed of 2000 rpm is a largely comparable knock limited operating point.
Figure 3.14 illustrates the dependency of the flame duration, the inflammation delay and the heat release on the geometric A/V-ratio. Discussed are the already known Pre-Chamber configurations (for academic purposes) coming with different shapes and spark locations. With a spark location of S=3.5 mm, the combustion is decelerated with an increasing orifice cross section area. The optimal A/V-ratio for a fast heat release is shifted to a lower A/V-ratio range from 0.025 to 0.04 compared to low pressure and temperature conditions, which was discussed in chapter 3.3. For elevated spark locations (S=10.0 mm and S=16.4 mm) the flame duration T10%-T70% reaches its minimum in the same A/V range 0.04 to 0.06. This is in accordance with the findings in chapter 3.3 for low pressure ignition conditions. It might be expected, that the turbulence production by the reacting jets during the inflammation and early flame propagating phase is independent of the ignition pressure. The main causes for the turbulence production are the orifice cross section area, the Pre-Chamber volume and indirectly the spark location. An increased Pre-Chamber volume produces a higher PC pressure rise and thus energy-richer and more persistent jets entering the main chamber. This enables short flame durations for elevated spark locations.

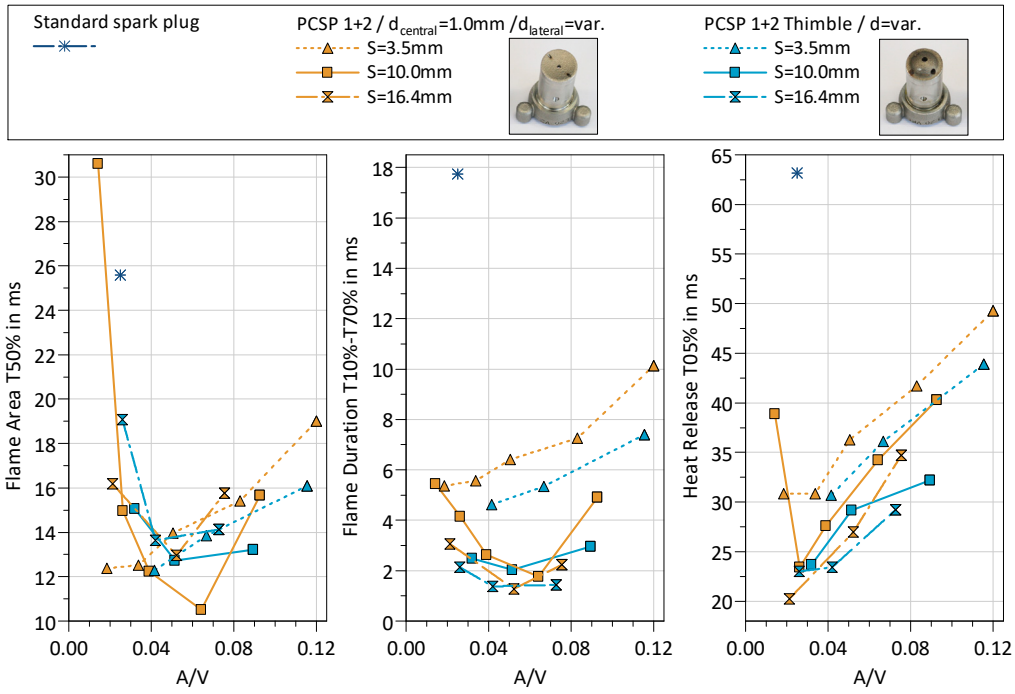

Figure 3.14: Impact of the overflow channel cross section area and spark location on the thermodynamic heat release and the flame propagation for different PCSP configurations in comparison to the standard spark plug ignition system. Ignition pressure p=18 bar. Equivalence-ratio ϕ=1.

The shortest inflammation delay (Flame at T50%) is achieved by an intermediate spark location S=10.0 mm in combination with a central orifice diameter $d_{central}$=2.5 mm. An extremely small A/V=0.014 in combination with tiny bore diameters d=1.0 mm increases the inflammation delay significantly and thus decelerates the speed of combustion. The inflammation probability for this particular design is smaller than 50%.
Figure 3.15 illustrates the influence of the orifice layout on the flame formation, the jet penetration and the heat release. In general, an increase of the orifice cross section area reduces the pressure rise inside the Pre-Chamber and decelerates the heat release in the main chamber. A reduction of A/V-ratio leads to an extremely elongated inflammation delay, but to a relatively fast heat release, caused by the jet ignition characteristics inside the main chamber. The two PCSP configurations, one with a large A/V=0.0093 (red line) and another one with a small A/V=0.026 (dark blue line) shows a comparable slope for the flame evolution, but causes a large temporal difference for the 5% of energy conversion. The smaller cross section area accelerates the main chamber heat release by 39%. In the single cylinder engine results in the previously published articles by Sens et al. [1, 24] it was stated, that a large orifice cross section area is disadvantageous in terms of high knock mitigation. A large area leads to a deceleration of the speed of combustion and thus to a retarded center of combustion with a reduced indicated efficiency. It can be concluded, that an optimal PCSP design for high engine loads requires an optimization of the cross section area and orifice diameter to solve the trade-off between a reliable inflammation, an acceptable ignition delay and a fast heat release.

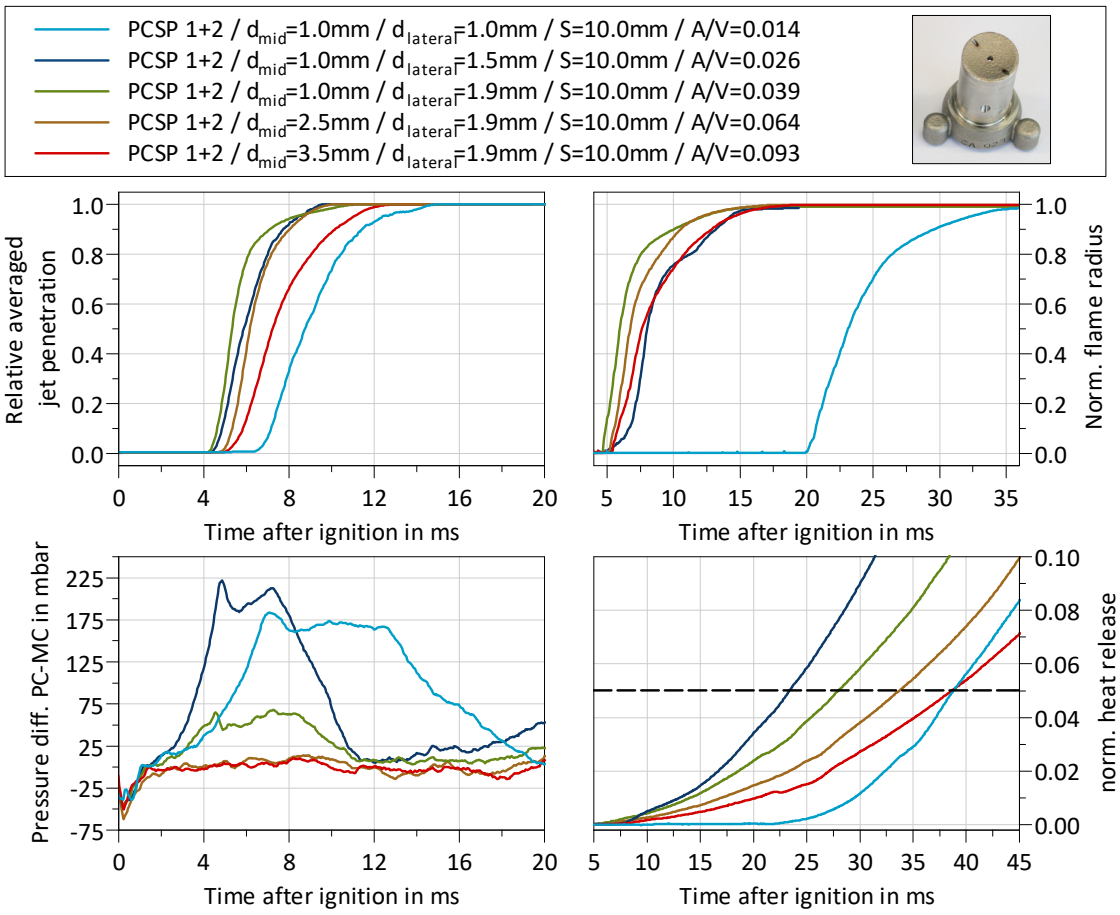

Figure 3.15: Impact of the geometric A/V-ratio on the flame evolution, jet penetration and heat release for 18 bar ignition pressure and an equivalence-ratio ϕ=1.

Figure 3.16 illustrates the influence of different bore layouts on the jet evolution and the inflammation inside the main chamber. The jet structure changes with an increasing central orifice diameter and cross section area from a typical open jet structure to a mushroom-shaped jet type. This corresponds to the findings in chapter 3.3 for low pressure ignition conditions. After the main chamber mixture has ignited and the flame propagates through the visible volume, the mushroom-shaped jet shows a reduced OH* intensity, which also correlates with the speed of heat release. Furthermore the flame ignition is initiated by the orifice with largest diameter. The OH* radicals and further combustion products stream into the main chamber and ignite the mixture in the vicinity of the jets centerline. This flame re-ignition process takes place in this region, because the early flame kernel development needs relative low turbulence intensities. Otherwise the developing flame will be distorted by the turbulent eddies, that enter into the flame structure. This characteristic reduces the turbulent mixing and thus minimizes the heat transport into the colder bulk gas. The pre-heat zone in front of the flame is small and supports the development of a self-sustainable flame front. For more details refer to the Borghi-Peters flame regime diagram in [32].
At lager stages, the highest OH* intensities are located at the significantly more turbulent shear layers, which enables a fast turbulent combustion process. A qualitative examination of the interaction of the jets shows that a larger overflow channel diameter causes larger spatial jet structures, which interact at earlier timings with each other. The turbulence level in these shear areas increases and retard locally the flame front development. It is expected, that a greater jet separation by wider overflow channel angles could improve the spatial inflammation and speed up the flame propagation.
The jet ignition process by hot gases away from the orifice could be observed for the PCSP configuration with the smallest cross section area. The flame extinguishes completely when passing the overflow channels. There is no detection of any OH* radicals exiting the orifices. The inflammation is significantly retarded. This finding is in accordance to the results of Biswas et al. [25]
In contrast to the flame ignition process, the formation of the flame front occurs first at the high turbulent shear layer as island shaped flame kernels at the left jet. The retarded ignition of the middle jet shows the same characteristic. The jet ignition can be described as a self-ignition inside the bulk gas, due to sufficient local thermodynamic and fast chemical pre-reactions. The measurement methodology does not allow to identify the specific reason for the local inflammation phenomenon in a reliable way. It is suggested, that the heat transport provides enough activation energy for starting chain branching reactions. An additional explanation is, that intermediate combustion products transported by the hot jets support the pre-reactions and thus the initiation of the heat release.
It was found that a strict separation in flame jet ignition or hot gas jet ignition regime might be difficult in some cases. The ignition process of the PCSP with an A/V=0.026 suggests, that the inflammation is very likely to be a combination of both processes. Beginning at 6.5 ms after ignition, very weak OH* radical intensities are observed at the larger lateral orifices. The radical emissions occur arbitrary and with random intensities at the exit of the lateral orifices. Later on, the OH* radicals capture a growing space along the center axis of the jet and produce spatially distributed inflammation kernels, which grow into the jet shear layer and accelerate the flame propagation accompanied by high OH* radical intensities.

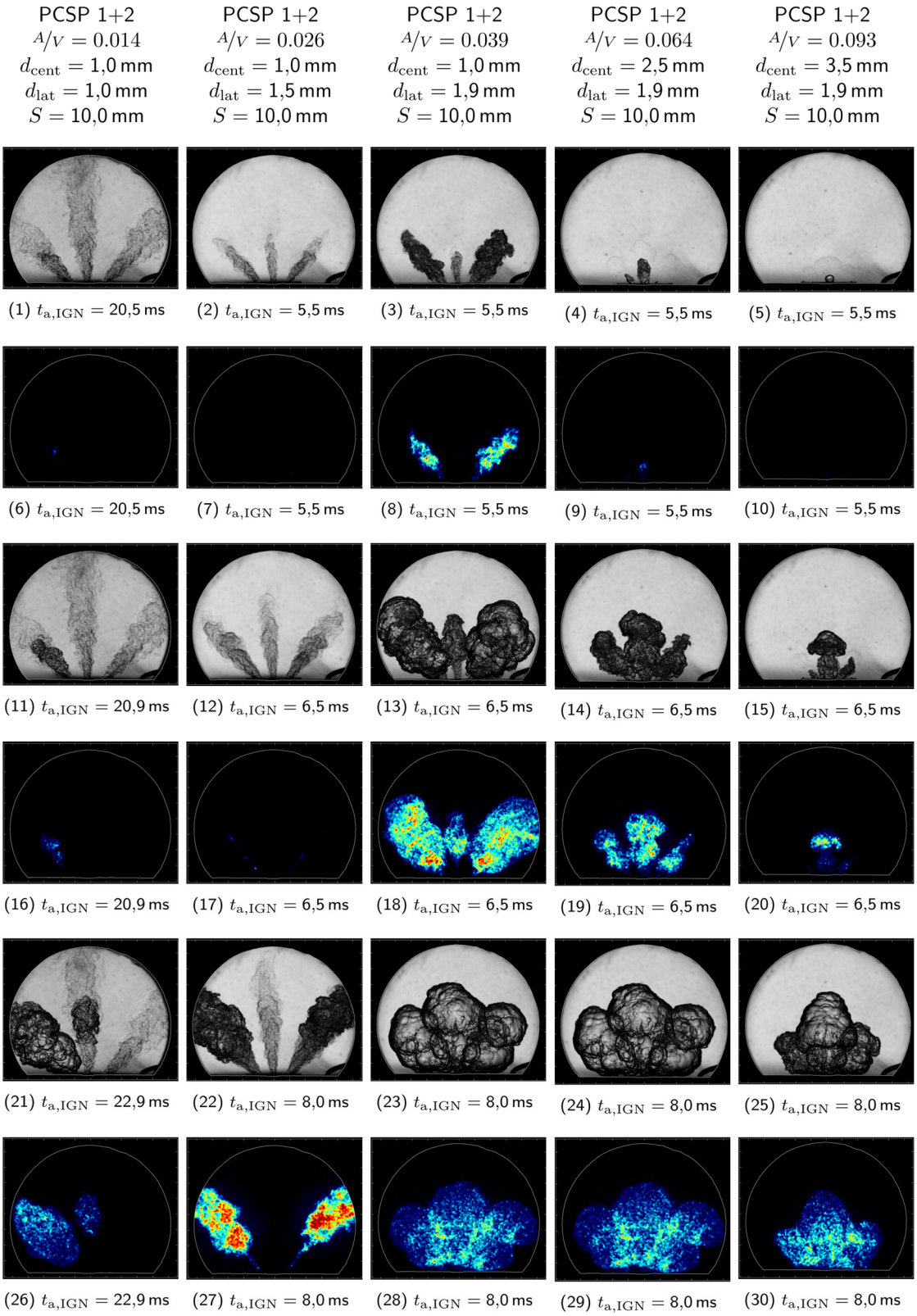

Figure 3.16: Impact of the overflow channel cross section area on the flame propagation for different PCSP configurations. Ignition pressure p=18 bar. Equivalence-ratio ϕ=1.

4 Conclusion and next steps

In order to build a deep understanding of Pre-Chamber based inflammation mechanisms, experiments in a combustion vessel with methane/air mixtures were carried out in varying boundary conditions in terms of chamber pressure, equivalence-ratio and geometrical design parameters of the Pre-Chamber. In order to quantify and compare the combustion characteristics with differing boundaries, both pressure measurements within the Pre-Chamber and main chamber as well as simultaneous Schlieren and OH* chemiluminescence measurements were performed and analyzed by means of morphological image analysis.
Here is a summary of the most vital findings:

- Based on the measurement principle of simultaneous Schlieren and OH* chemiluminescence, three different ignition mechanisms inside the main chamber could be observed: ignition by a reacted jet (“hot gas jet ignition”), ignition by a reacting jet (“flame jet ignition”) as well as a combination of both.
- The vast majority of combustion events inside the main chamber can be attributed to a flame jet ignition, while only two cases at lowest vessel pressure of 3 bar and smallest orifice diameter indicate the presence of a pure hot gas jet. One of the two hot jet cases fails to ignite the main chamber at 3 bar.
- There is only one case at 18 bar showing a distinct hot gas jet ignition at 18 bar vessel pressure. This case is characterized again by minimum orifice diameter and absolute minimum A/V ratio and leads to an overly long inflammation delay. However, the initial heat release is very fast, which can be attributed to the nature of auto-ignition like combustion progress for the hot gas jet ignition.
- The pressure dependency of flame propagation / combustion speed is drastically reduced in the quiescent vessel conditions with the Pre-Chamber spark plug compared to conventional ignition. This is mainly due to the deep and fast penetration of the jets which consequently results in a spatial inflammation inside the main chamber. Above this, the high jet velocity induces a high level of turbulence by its own, which both temporally and spatially serves perfectly for an additionally accelerated flame propagation. It needs to be stated though, that if local turbulence gets too high in additionally poor mixture conditions, specifically the hot gas jet regime might lead to misfire in the main chamber. Nevertheless, these PCSP inherent features of spatial ignition and self-generated turbulence make the PCSP a particularly good match for high engine load and knock mitigation.

Based on these fundamental investigations, findings from previous single cylinder engine experiments are supported and understood in more detail. The single impact, importance and interference of the varied parameters and their effect onto combustion is widely understood, which is a necessity for the dedicated layout of the Pre-Chamber. The work described in this publication is then also the point of departure for setting up a detailed combustion model in 3D CFD, which needs to be capable of predicting the phenomena discussed within this paper in order to efficiently design the optimum compromise layout and address properly all the challenges for the PCSP in rather poor ignition conditions such as low mixture temperature and low cylinder pressure.

5 Literature

[1] SENS, M., E. BINDER, A. BENZ, et al: *Pre-Chamber Ignition as a Key Technology for Highly Efficient SI Engines - New Approaches and Operating Strategies,* 39th International Vienna Motor Symposium, Vienna, 2018.

[2] GUETHE, F., D. GUYOT, G. SINGLA, N. NOIRAY, B. SCHUERMANS: *Chemiluminescence as diagnostic tool in the development of gas turbines*, Applied Physics, 2012.

[3] JENS, E.T., V.A. MILLER, B.J. CANTWELL: *Schlieren and OH* chemiluminescence imaging of combustion in a turbulent boundary layer over a solid fuel*, Experiments in Fluids 57(3):39, 2016.

[4] SOID, S.N., Z.A. ZAINAL: *Spray and combustion characterization for internal combustion engines using optical measuring techniques – A review*, Energy, Elsevier, vol. 36(2):724-741, 2011.

[5] LAUER, M., T. SATTELMAYER: *On the Adequacy of Chemiluminescence as a Measure for Heat Release in Turbulent Flames With Mixture Gradients,* Proceedings of the ASME Turbo Expo, Orlando, 2009.

[6] JIPPA, K.-N.: *Onlinefähige, thermodynamikbasierte Ansätze für die Auswertung von Zylinderdruckverläufen*, Schriftenreihe des Instituts für Verbrennungsmotoren und Kraftfahrwesen der Universität Stuttgart, Expert Verlag, 2004.

[7] WARNATZ, J., U. MAAS, R.W. DIBBLE: *Combustion: Physical and chemical fundamentals, modeling and simulation, experiments, pollutant formation,* 4th ed., Springer, Berlin, 2006.

[8] ALEIFERIS, P.G., A.M.K.P. TAYLOR, J.H. WHITELAW, K. ISHII, Y. URATA: *Cyclic Variations of Initial Flame Kernel Growth in a Honda VTEC-E Lean-Burn Spark-Ignition Engine*, SAE Paper 2000-01-1207, 2000.

[9] ALEIFERIS, P.G., A.M.K.P. TAYLOR, J.H. WHITELAW, K. ISHII, Y. URATA: *The nature of early flame development in a lean-burn stratified-charge spark-ignition engine*, Combustion and Flame, 136(3), 283-302, 2004.

[10] BADAWY, T., X. BAO, H. XU: *Impact of spark plug gap on flame kernel propagation and engine performance*, Applied Energy, 191, 311-327, 2017.

[11] GOSCHÜTZ, M., M.S. MOHD SHAWAL, M. SCHILD, C. SCHULZ, S. KAISER: *Comparison of flame-front visualization in internal combustion engines using different imaging systems via endoscopic and full optical access*, 7th European Combustion Meeting, Budapest, 2015.

[12] GOSCHÜTZ, M., C. SCHULZ, S. KAISER: *Endoscopic Imaging of Early Flame Propagation in a Near-Production Engine*, SAE International Journal of Engines, 2014.

[13] SHAWAL, S., M. GOSCHÜTZ, M. SCHILD, S. KAISER, M. NEUROHR, J. PFEIL, T. KOCH: *High-Speed Imaging of Early Flame Growth in Spark-Ignited Engines Using Different Imaging Systems via Endoscopic and Full Optical Access*, SAE Int. J. Engines, 9, 704-718, 2016.

[14] ABU-GHARABIEH, R., G. HAMARNEH, T. GUSTAVSSON, C.F. KAMINSKI: *Flame front tracking by laser induced fluorescence spectroscopy and advanced image analysis*, Optics Express, 8(5), 278, 2001.

[15] ABU-GHARABIEH, R., C. KAMINSKI, T. GUSTAVSSON, G. HAMARNEH: *Flame front matching and tracking in PLIF images using geodesic paths and level sets*, IEEE Workshop on Variational and Level Set Methods in Computer Vision, Proceedings, Vancouver, Canada, 13 July 2001.

[16] MALM, H., G. SPARR, J. HULT, C.F. KAMINSKI: *Nonlinear diffusion filtering of images obtained by planar laser-induced fluorescence spectroscopy*, Journal of the Optical Society of America A, 17(12), 2148, 2000.

[17] PARK, D.J., A.R. GREEN, Y.C. CHEN: *Analysis of Local Flame Propagation in Gas Explosions with Multiple Obstacles*, 15th Australasian Fluid Mechanics Conference.

[18] PARSINEJAD, F., J.C. KECK, H. METGHALCHI: *On the location of flame edge in Shadowgraph pictures of spherical flames - A theoretical and experimental study*, Experiments in Fluids, 43(6), 887-894, 2007.

[19] SILJAN, E., M. LYSAKER, S. MAHARJAN: *Wave Front Tracking using Template Matching and Segmented Regression*, Linköping University Electronic Press, S. 326-331, 2017.

[20] YANG, X., X. SHEN, J. LONG, H. CHEN: *An Improved Median-based Otsu Image Thresholding Algorithm*, AASRI Procedia, 3, 468-473, 2012.

[21] OTSU, N.: *A Threshold Selection Method from Gray-Level Histograms*, IEEE Transactions on Systems, Man, and Cybernetics, 9(1), 62-66, 1979.

[22] SETTLES, G.S.: *Schlieren and Shadowgraph Techniques: Visualizing Phenomena in a Transparent Media*, Berlin Heidelberg, Springer-Verlag, 2001.

[23] SMITH, G.P., D.M. GOLDEN, M. FRENKLACH, N.W. MORIARTY, B. EITENEER, M. GOLDENBERG, C.T. BOWMAN, R.K. HANSON, S. SONG, W.C. GARDINER, V.V. LISSIANSKI, Z. QIN: http://www.me.berkeley.edu/gri_mech/

[24] SENS, M., E. BINDER, P.B. REINICKE, M. RIEß, M. WÖBKE: *Pre-Chamber ignition and promising complementary technologies*, 27th Aachen Colloquium Automobile and Engine Technology, Aachen, 2018.

[25] BISWAS, S., S. TANVIR, H. WANG, L. QIAO: *On ignition mechanisms of premixed CH_4/air and H_2/air using a hot turbulent jet generated by pre-chamber combustion*, Applied Thermal Engineering, Volume 106, 2016.

[26] SUCKART, D., D. LINSE, E. SCHUTTING, H. EICHLSEDER: *Experimental and simulative investigation of flame–wall interactions and quenching in spark-ignition engines*, Automotive and Engine Technology, 2(1), 25-38, 2017.

[27] HASSE, C., M. BOLLIG, N. PETERS: *Quenching of laminar iso-octane flames at cold walls*, Combust. Flame 122, 117–129, 2000.

[28] XIAO, H., R.W. HOUIM, E.S. ORAN: *Formation and evolution of distorted tulip flames*. Combustion and Flame, 162(11), 4084-4101, 2015.

[29] XIAO, H., Q. WANG, X. SHEN, S. GUO, J. SUN: *An experimental study of distorted tulip flame formation in a closed duct*, Combustion and Flame, 160(9), 1725-1728, 2013.

[30] PONIZY, B., A. CLAVERIE, B. VEYSSIÈRE: *Tulip flame - the mechanism of flame front inversion*, Combustion and Flame, 161(12), 3051-3062, 2014.

[31] LEE, S., C. BAE, R. PRUCKA, G. FERNANDES, Z. FILIPI, D.N. ASSANIS: *Quantification of Thermal Shock in a Piezoelectric Pressure Transducer*, SAE International, 2005.

[32] PETERS, N.: *Combustion Theory*, CEFRC Summer School, 184-194, Princeton, 2010

6 Abbreviations and formula symbols

A/V	Ratio of Pre-Chamber orifice cross section area to volume
BMEP	Brake mean effective pressure
CA	Crank Angle
CA50	Center of heat release
CFD	Computational Fluid Dynamics
CH_4	Methane
CO_2	Carbon dioxide
CR	Geometric compression ratio
d	Bore diameter
d_{cent} / $d_{central}$	Diameter of the central bore
d_{lat} / $d_{lateral}$	Diameter of the lateral bore
ECU	Engine control unit
EGR	Exhaust gas recirculation
EIVC	Early intake valve closure
fps	Frames per second
GRI3.0	Reaction mechanism with 53 species
HEV	Hybrid Electric Vehicle
ICE	Internal combustion engines
IGN	Ignition timing
MBT	Maximum Break Torque

NIST	National Institute of Standards and Technology
N_2	Nitrogen
O_2	Oxygen
OH / OH*	Hydroxide (exited)
PC	Pre-Chamber
PCSP	Pre-Chamber spark plug
PHEV	Plug-in Hybrid Electric Vehicle
RPM	Revolutions per minute
S	Spark gap location inside the PCSP
T10%/T50%/T70%	Time where flame area covers 10%/50%/70% of visual field
$t_{a,IGN}$	Time after ignition
TDC	Top dead center
UV	Ultra violet
xHEV	Hybrid Electric Vehicle with light electrification

Acknowledgement

The authors thank all IAV colleagues who showed tremendous dedication in making this paper such a success. A special mention in this regard goes to Jonas Roswag, Annett Kunze and Emanuel Binder.
The authors thank also the support provided by Lars Alberding, Alexander Pauls and Prof. Dr.-Ing. Peter Eilts from the institute for internal combustion engines of the technical university Braunschweig.